Propagating and Combining Aleatory Uncertainties characterized by Continuous Random Variables and Sparse Discrete Realizations from Random Functions[1]

Vicente J. Romero

V&V, UQ, Credibility Processes Dept.

Sandia National Laboratories,[2] Albuquerque, NM

Abstract

This paper presents a practical methodology for propagating and combining the effects of random variations of several continuous scalar quantities and several random-function quantities affecting the failure pressure of a heated pressurized vessel. The random functions are associated with stress-strain curve test-to-test variability in replicate material strength tests (uniaxial tension tests) on nominally identical material specimens. It is demonstrated how to effectively propagate the curve-to-curve discrete variations and appropriately account for the small sample size of functional data realizations. This is coordinated with the propagation of aleatory variability described by uncertainty distributions for continuous scalar quantities of pressure-vessel wall thickness, weld depth, and thermal-contact factor. Motivated by the high expense of the pressure vessel simulations of heating, pressurization, and failure, a simple dimension- and order-adaptive polynomial response surface approach is used to propagate effects of the random variables and enable uncertainty estimates on the error contributed by using the surrogate model. Linear convolution is used to aggregate the resultant aleatory uncertainty from the parametrically propagated random variables with an appropriately conservative probability distribution of aleatory effects from propagating the multiple stress-strain curves for each material. The response surface constructions, Monte Carlo sampling of them for uncertainty propagation, and linear sensitivity analysis and convolution procedures, are demonstrated with standard EXCEL spreadsheet functions (no special software needed).

---

[1] Sandia National Laboratories document SAND2019-zzzz C. This paper is a work of the United States Government and is not subject to copyright protection in the U.S. This manuscript describes objective technical results and analysis. Any subjective views or opinions that might be expressed in the paper do not necessarily represent the views of the U.S. Department of Energy or the United States Government.

[2] Sandia National Laboratories is a multi-mission laboratory managed and operated by National Technology and Engineering Solutions of Sandia, LLC., a wholly owned subsidiary of Honeywell International, Inc., for the U.S. Department of Energy's National Nuclear Security Administration under contract DE-NA0003525.

1. Introduction

This paper presents a practical methodology for propagating and combining the effects of random variations of several continuous scalar quantities and several random-function quantities affecting the failure pressure of a heated pressurized vessel. The random functions are associated with stress-strain curve variability from test-to-test in replicate material strength tests (uniaxial tension tests) on nominally identical round-bar material specimens.

A difficulty is that only a few material tests and derived stress-strain curves exist for each of several materials making up the pressure vessel. Substantial difficulties are encountered when using spectral methods to try to infer or model, from just a few experimentally observed stress-strain curves, the governing random function from which the experimental variations emanate (e.g., see the appendix of [1]). This is not surprising, as even the much simpler problem of appropriately inferring or modeling a scalar quantity's aleatory probability distribution from just a few samples or realizations of the scalar quantity is itself a very difficult proposition (e.g., [1]-[6]). This paper demonstrates how to effectively overcome this limitation and propagate the curve-to-curve variations and appropriately account for the small sample size of functional data realizations.

This methodology is coordinated with the need in the present problem to propagate and combine the effects of aleatory variability of pressure-vessel scalar quantities of wall thickness, weld depth, and thermal-contact effectiveness factor. Motivated by the high expense of the pressure vessel simulations of heating, pressurization, and failure, a simple dimension- and order-adaptive polynomial response-surface surrogate model is used for inexpensive Monte Carlo propagation of the effects of the mentioned parametric scalar uncertainties. The upgradable response surface also enables uncertainty estimates on the error contributed by using the surrogate model.

Then linear convolution is used to aggregate the resultant aleatory uncertainty from the parametrically propagated random variables with an appropriately conservative probability distribution of aleatory effects from propagating the various stress-strain curves for the materials. The convolution methodology was developed and first applied in a verification, validation, and uncertainty quantification (VVUQ) methodology advancement project [7] involving the heated pressurized vessel. The convolution methodology has since been successfully used also in a complex structural-dynamics model calibration and VVUQ problem at Sandia National Laboratories.

Sensitivity analyses are also performed in the present paper to assess the relative contributions of the parametric and discrete uncertainty sources on the total variability of predicted failure pressure.

Various aspects of the heated-pressurized-vessel VVUQ problem and associated methodology are described in [7] – [14] and the present paper. The modeling and VVUQ activities were performed under a multi-year "abnormal thermal-mechanical breach" (T-M breach) task [7] of a Predictive Capability Assessment Project (PCAP) in the Verification & Validation (V&V) sub-element of the U.S. Dept. of Energy Advanced Simulation and Computing (ASC) program. The goal of the PCAP T-M breach task was to assess the error and quantify the uncertainty in modeling the thermal-chemical-mechanical response and weld related breach failure of sealed canisters ("cans") weakened by high temperatures and pressurized by heat-induced pyrolysis of foam. The planned outcome of the PCAP T-M breach task was to measure improvements in prediction accuracy over time as the models and computer platforms became more capable.

The Sandia Weapon System Engineering and Assessment Technology Campaign (WSEAT) program supported the PCAP project by conducting material characterization tests [13] and validation experiments [14][1] (see Figure 1). This partnership provided an opportunity to develop a fully integrated process from design of experiments through model validation assessment, with uncertainty reduced as much as possible and propagated through the process.

Figure 1. Thermal-chemical-mechanical validation experiments [14], including internal pressure response. The 'can' includes the cylindrical 'sidewalls' or 'walls', as well as the top 'lid' and bottom 'base'.

Breach failures were expected to occur, and in the tests did occur, at the circumferential perimeter (laser) weld that joins the top lid to the can sidewalls. This is because the weld thickness is significantly less than the can lid and sidewalls (see Figure 2), and the tests/cans of interest in this paper were radiatively heated at the lid top surface, so the top weld material was much hotter/weaker than the perimeter weld material at the bottom or base of the can. While prediction of canister internal temperatures, time to breach, and breach pressure are sought in the T-M breach task, breach pressure is the quantity of interest (QOI) in this paper.

Section 2 of this paper summarizes the physics models used for predicting can thermal, pressurization, and structural response (and failure). Selected physics model simulations are used to populate adaptive polynomial response-surface surrogate models as described in section 3. Their use for inexpensive Monte Carlo propagation of the parametric aleatory uncertainties is described, as are surrogate-related error estimates that the upgradable response surfaces enable. Selected simulations with the physics model are used to propagate the various stress-strain curves as described in Section 4. Section 5 describes the convolution procedure for aggregating the resultant aleatory response (pressure breach failure) uncertainties obtained in sections 3 and 4. Sensitivity analyses regarding the various contributors to uncertainty are presented in sections 3 - 5. Section 6 provides some summary observations and conclusions.

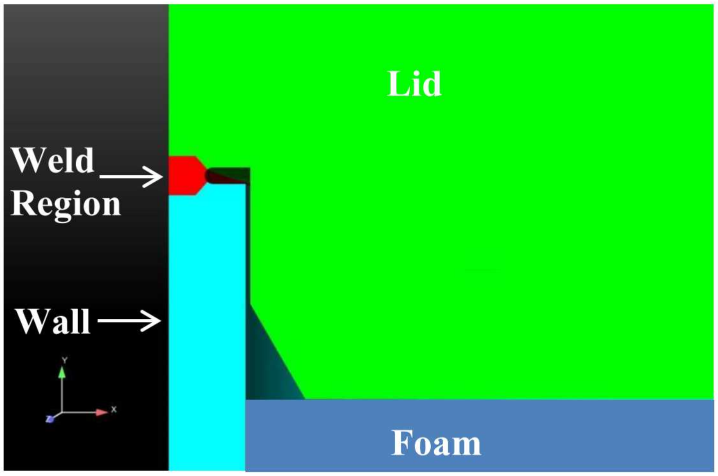

Figure 2. Closeup of modeled geometry where can top lid, sidewall, and internal foam meet. (Nominal geometry values are 0.03 in. weld depth, 0.0645 in. wall thickness, and 0.007 in. clearance between the lid and side wall in the weld region.) Figure from [7].

2. Thermal-Chemical-Mechanical-Failure Models of Heated Pressurizing Can Response and Failure

2.1 Material Tension Tests and Stress-Strain Constitutive Model

The material tension tests and results, strength constitutive model, and material damage models and failure criteria are briefly summarized here from references [7] and [1]. These provide much more detailed information.

The material characterization tests involve uniaxial tension tests on several cylinder specimens at each of seven temperatures spanning the 800C temperature excursion experienced by the heated can, for two stainless-steel alloys that make up the can materials. Reference [13] provides information on the material testing equipment and procedures.

Nominal strain rates of 0.001/s were used in the tension tests. This strain rate was based on model-predicted conditions in the PCAP thermal-mechanical breach experiments [1]. A strain rate of 0.0001/s, based on computed local strain rates in the weld region, was also tested to explore the sensitivity of the material to strain rate. However, strain-rate effects were not included in the PCAP material strength model because it was figured that in the accident scenarios being assessed, strain-rate effects were of secondary importance prior to reaching a stress-strain maximum load condition where our failure criteria would be activated (see next subsection). For conditions past maximum load, it is well known that 304L stainless steel (ss) has non-negligible strain-rate dependence at all temperatures.

The test results for the PCAP can lid and base material are shown in Figure 3 in terms of engineering stress versus engineering strain. As expected, the strength of the material decreases as the temperature increases. However, around 600ºC there is a noticeable inflection point in the temperature related shape trend of the stress-strain curves. It is believed that this inflection occurs because the deformation mechanisms change from void growth and deformation to grain slippage at about half of the material melt temperature which is roughly 700ºC for 304L stainless steel.

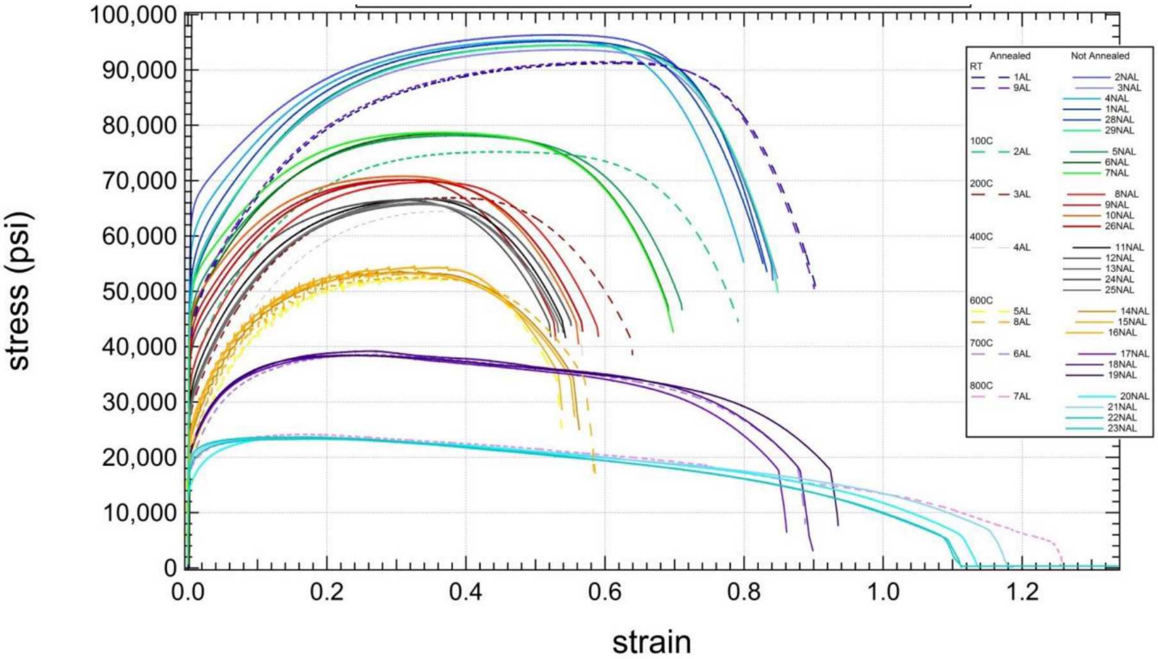

Figure 3. Example of engineering stress vs engineering strain curves for PCAP lid and base material (ss 304L). Figure from [9], [13].

The test results for the PCAP wall material are found in [7], [1]. Like the lid material, the strength of the wall material decreases as the temperature increases and a noticeable change in the temperature related shape trend of the stress-strain curves occurs at about 600ºC.

Mechanical constitutive behavior is modeled using a strain-rate-independent isotropic ductile-metal Multi-Linear Elastic Plastic (MLEP) plasticity model (e.g., [9], [15]). Creep effects were not considered but are thought to be immaterial to the material response prediction scenarios of interest. Other fundamental assumptions of the MLEP model are summarized in, e.g., [9]. The MLEP model is a standard metal plasticity constitutive representation for industry practice. It helps FE models be affordable with reasonable computational resources and is suitable as long as the limitations are understood and not violated significantly. The MLEP model only relates stress and strain; no intrinsic statement about material strength related failure is made. Material failure modeling is discussed in the next subsection.

The parameterized form of the MLEP-specific stress-strain curve (Cauchy stress – plastic logarithmic strain) is represented in piecewise linear fashion by multiple linear segments. This parameterization involves solving sequential inverse problems to determine in a step-wise manner the MLEP stress–strain curve segments that best recover the load-displacement or engineering stress-strain curve (e.g. Fig. 3) from the tensile tests. A fitting procedure described in [9] (following [39]) was used to enable the inverse calculation. Several factors that influence the success of the iterative MLEP procedure are described. The differences between MLEP curves calibrated to different nominally identical tests/specimens were much larger than the fitting errors in the calibrations.

Before the onset of specimen necking in a tension test, the MLEP stress and strain values can be calculated from the load-displacement recorded from the load cell of the testing frame and an extensometer mounted on the specimen. Once necking occurs, the true strain in the middle of the necked region must be calculated from a finite element (FE) model of the gage section of the specimen. The ASC massively parallel solid-mechanics code Adagio [16] was used for the simulations. To ensure that necking initiates between the ends of the gage section, a small imperfection is introduced in the mesh. Hex-mesh density effects were investigated and controlled to be negligible up to the material failure criterion point on the MLEP stress–strain curve corresponding to the maximum stress point on the experimental curve (see next subsection).

Since the test data contains a large number of potentially noisy data points, some data conditioning through down-sampling and/or smoothing is necessary, resulting in order ~20 data points (see [9]). This is based on engineering judgement.

2.2 Weld Material Modeling and Failure Criteria

It was originally planned to obtain weld material stress-strain curves and failure criteria by calibrating to tension tests of butt-weld square bar specimens and then validating to can pie-section weld flexure tests to failure. However, both endeavors proved to be problematic experimentally and computationally [7] such that adequate model accuracy could not be established.

As a reasonable alternative, the following approach was taken. For welds of normal quality that don't have anomalies like voids, empirical evidence strongly suggests that weld material strength lies somewhere between the strengths of the two materials joined by the weld—here the lid and the can wall. Wall/tube material was slightly weaker at max load than the lid/bar-stock material, so a conservative-leaning choice was made to assign the wall/tube material curves and failure criteria to the weld.

Microstructural examination of the PCAP cans pressurized to failure indicated ductile overload failure at the laser welds of the heated lids. As described in [9], Equivalent plastic strain (EQPS) and tearing parameter (TP) are candidate models for accumulated material damage. These models' computed damage values at the point of maximum engineering stress in the uniaxial tension tests are taken to be critical material failure levels for these two models. This is consistent with current failure modeling practice at Sandia in conjunction with MLEP models in overload failure modes. Because of the notorious difficulty of predicting structural failure from material damage modeling, the two models and their failure criteria were used and assessed as candidate indicators of onset of structural failure in the PCAP application.

Although TP and EQPS critical values are often defined based on tension test material separation failure, the critical values for this project were defined at the maximum load in the tension tests. This decision was made for two reasons. First, the global loading of the can structure is due to pressurization, and the pressure is always increasing and will cause incipient failure when a maximum load condition is reached. Second, the weld failures observed in the can tests showed little evidence of necking. Up to maximum load there is little necking. It was reasoned that defining critical failure values based on any finite element in the model reaching the hardening curve maximum load point identified from the tension tests would result in conservative failure predictions for the can.

Hence, the failure criteria defined at the maximum load in the tube/wall round bar tension tests were used to signify weld material failure in the can breach predictions. The failure criteria values are given in [9] for each tube/wall stress-strain curve at the tested temperatures.

2.3 Models for Can Thermal-Chemical-Structural Response and Failure

The thermal-chemical-mechanical models used are briefly summarized next from [7]. The Sandia SIERRA module [18] for massively parallel thermal-fluid computations was used to model the heating of the can, its thermal response, and thermally-induced chemical-kinetic decomposition of the foam [19] and resulting gas species generation that causes pressurization. The solid mechanics and structural modeling module [16] was used to model the mechanical response of the can and failure at the weld under quasi-static pressurization and high temperatures and large temperature variations in time and space.

The thermal-chemical simulation provides the temperature and pressure boundary conditions for the mechanical model. The only feedback from the mechanical model to the thermal-chemical model is the can's internal volume change due to deformation. The volume change affects the pressure level in the can through the Ideal Gas Law which is evaluated within the thermal module and then communicated to the mechanical module. The can geometry is not changed/updated in the computational heat-transfer model because the can deformation is fairly slight (lateral bulging equivalent to a few can-wall widths) so is thought to negligibly affect the heat transfer (or at least not affect the heat transfer in the model, given the way it was modeled). The heat transfer and foam decomposition submodels and parameters are also not affected by pressure in the current treatment. (The uncertainties associated with including pressure effects on these phenomena were judged larger than the error involved by not including pressure effects, and any modeling error effects would be quantified through the validation comparisons ([7], [1]) that were the culmination of the PCAP assessments.)

The thermal-chemical and mechanical models were run in a "concurrent but segregated" manner in which Sandia's SIERRA [20] software framework for massively parallel multi-physics computations passed temperature, pressure, and volume information between the thermal-chemical simulation and the mechanical simulation. SIERRA coordinates and manages the different time-stepping of the thermal-chemical and mechanical codes and the transfer of spatial temperature fields solved on the tetrahedral thermal mesh to nodal temperature assignments to the nodes of the mechanical hex mesh.

The full 360-degree can geometry with internal foam was used for the thermal-chemical simulations and a 90-degree pie-slice geometry without foam was used for the mechanical simulations. A full 360-degree geometry was used in the thermal-chemical simulations because at the time, the foam and enclosure radiation models didn't accommodate any kind of symmetry boundary conditions. The mechanical simulations were much more computationally expensive, so a quarter-can partial geometry without foam was used to reduce cost. Leaving foam out of the mechanical model tremendously reduces the number of finite elements and thus computational cost, and is thought to have negligible impact on structural behavior and pressure-breach failure in the PCAP problem.

In the thermal model, a uniform heat flux boundary condition was applied on the lid surface. The flux level was calculated as follows to be consistent with the temperature data from the experiment control TCs. The four control TCs were fully inserted into radially drilled holes at midplane on the lids at 0, 90, 180, and 270 degrees around the lids [14]. A Proportional-Integral-Derivative (PID) routine [21] was used to determine the heat flux magnitude needed to match the control thermocouple temperature responses. This approach results in a more realistic temperature distribution versus using a TC-guided uniform temperature condition over the entire lid surface. On the side walls and base of the can, convection and radiation boundary conditions were specified (as described in [10]) to represent the heat transfer between the can exterior and the surrounding environment.

Different element types and mesh densities are used as appropriate in the thermal and mechanical models [7]. Code verification activities were performed for the thermal and solid/structural mechanics codes and models ([7]). For the order-200 thermal-mechanical and mechanical-only simulations run for VVUQ and sensitivity analysis in the PCAP project, an affordable mesh size of 1.85 million hex elements for the structural model (12 elements through the thickness of the weld) and 14.3 million tet elements for the more affordable thermal model were used. This affordable 'Level 4' mesh was one in a succession that went up to Level 6 with approximately double the number of elements in the structural and thermal models (see [8]). The succession of meshes was used for a solution verification assessment in [7][1] to estimate and account for Mesh 4 related error/uncertainty in the VVUQ analysis and results in [12]. Solver tolerances were experimented with and set to contribute small error/uncertainty relative to mesh effects.

Figure 4 shows the Level 4 mesh at a critical portion of the structural model where weld failure is determined in the thermal-structural simulations. Stress concentration is evident at the crown of the weld notch. This type of weld geometry representation was found to best support weld failure predictions, from analyzing many different geometry representation schemes ([17], [7]).

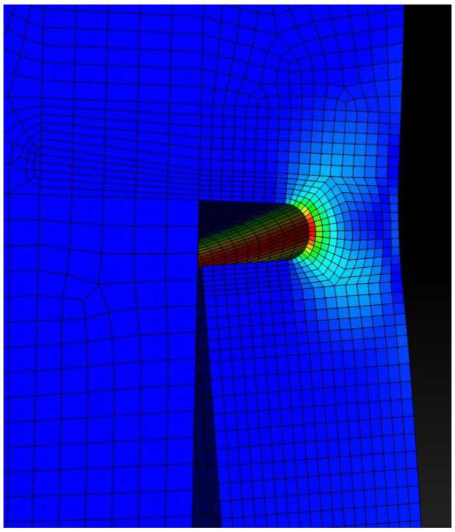

Figure 4. Weld-section closeup of structural-model Level 4 hex mesh used in the model validation, UQ, and sensitivity analysis simulations in the PCAP project. Stress concentration is evident at the crown of the weld notch. (Figure from [8].)

3. Parametric Propagation of Aleatory Random Variable Inputs to Can Breach-Pressure Variability Predictions

The breach pressure predictions are intended to estimate failure pressure variability in an asymptotically large population of cans having small can-to-can variations characteristic of measured or inferred variations in five actual cans (nominally identical) experimentally tested to failure [14]. Experimental failure pressures are to be compared against predicted failure pressures in a model validation assessment. For proper validation comparisons, the test-to-test and can-to-can aleatory variations in the experiments and simulations must be properly treated, as well as the systematic or epistemic uncertainties in the experiments and simulations. An uncertainty accounting system for processing experimental and model/simulation aleatory and epistemic uncertainties for the purpose of model validation comparisons is explained and illustrated in [12] for the PCAP application. The uncertainty propagation and aggregation methods and results in the present paper as well as [10], [11] feed into the model validation assessment in [12]. Careful characterization of the uncertainties to be treated is essential. This is documented in [7] - [14].

We state from [7] the can-to-can variability ranges estimated from experimental measurement data and mod-sim analysis for the random variables parametrically propagated in this section.

- **weld depth, *d***: variation between reasonable limits of [0.023 *in*, 0.031 *in*], to be treated as a uniform distribution
- **wall thickness, *t***: variation between reasonable limits of [0.062 *in*, 0.0645 *in*], to be treated as a uniform distribution
- **lid thermal contact effectiveness factor, *f***: variation between reasonable limits of [20%, 90%] of the way between extremes of no heat transfer and perfect-contact heat

transfer across the vertical and horizontal sections of the gap between lid and wall in Figure 2, to be treated as a uniform distribution between 20% and 90%.

Note that wall flexibility was reasoned to potentially have a non-negligible effect on maximum stress at the weld, and thus on the pressure level at which failure is predicted. Wall flexibility is affected by both wall thickness and temperature of the wall (the latter is non-negligibly affected by the gap heat transfer from the lid which was radiatively heated in the validation experiments being modeled). Of course, weld depth non-negligibly affects predicted failure pressure.

The other prominent aleatory uncertainties in the PCAP problem are the material stress-strain curves for the can lids, weld, and wall. These uncertainties come in the form of ***discrete*** uncertainty information (not parametric) and are addressed in the next section. The parametric uncertainties in this section are evaluated conditional on nominal median-strength stress-strain curves used for the can lids, weld, and wall as identified in the next section, and nominal values of the 13 other parametric uncertainties in the validation analysis (see [12]). The model (Mesh 4) was run with experimental heating and other conditions from Test 6, which is the reference nominal test (see [10]) of the five replicates in the PCAP validation assessment.

The remainder of this section describes the construction of dimension- and order- adaptive upgradable response-surface surrogate models used for inexpensive Monte Carlo propagation of the parametric uncertainties cited above. A key feature of the upgradable response surfaces is that they enable surrogate-related error estimation. Sensitivity analysis of the relative contributions of the various uncertainty sources to the total uncertainty is also presented.

Construction of 3D Linear Response Surface Approximation

Table 3-1 shows the equation sets and coefficient values for linear polynomial response surfaces of failure pressure as a function of the said parameters, for both TP and EQPS failure criteria. The linear polynomial response surface equation is written in the generic form $f(w1,w2,w3)$ presented in the table. To determine the equation's four coefficients b0 – b3, four versions of the equation are obtained by evaluating it at four different points in the three-dimensional (3D) *d-f-t* parameter space where response values are also computed with the computational physics model. These points are at four strategically selected "construction points" in the parameter space as discussed below. The system of four equations and four unknowns is solved to yield the values of the four coefficients. Then the equation provides a linear approximation to the physics model's output response variation over the parameter space and can be evaluated at any point (d, f, t) in the space to yield an approximate response value at points away from the four construction points (at the construction points, the RSA function exactly matches the physics model results).

In the present analysis, the physics model's nominal input values d^o, f^o, t^o (and the nominal values for the other model inputs, though those are not explicitly written in the following) comprise a reference point $\vec{z}^o$ in the parameter space of inputs to the physics model. Then a vector of input values $\vec{z}=[d, f, t]^T$ can be written as the sum of the reference values $\vec{z}^o = [d^o, f^o, t^o]^T$ and deviations $\vec{w}=[\Delta d, \Delta f, \Delta t]^T$ from the reference values:

$$\vec{z} = \vec{z}^o + \vec{w}. \tag{1}$$

The TP and EQPS polynomial RSAs $f(w_i)$ used in this study are written in terms of independent orthogonal coordinates $w1$, $w2$, and $w3$ that are respectively parallel with, and positively directed in the same directions as, the d, f, and t parameter space coordinates. The $w1$-$w2$-$w3$ coordinate frame origin is located at the reference nominal point $\vec{z}^o$ in the d-f-t parameter space, which has physics model input values (d^o, f^o, t^o) in the original coordinates, and RSA function input values (0,0,0) in the $w1$,$w2$,$w3$ translated coordinates. Any other point $\vec{z}^i$ in the input parameter space of the physics model, like the points selected for RSA construction, map to input parameter values $\vec{w}^i$ for the RSA function using a rearrangement of Eqn. 1:

$$\vec{w}^i = \vec{z}^i - \vec{z}^o. \qquad (2)$$

Because $\vec{z}^o$ is comprised of nominal physics model inputs, $\vec{z}^o$ is generally centrally located in the uncertainty region to be investigated. The construction points for the RSA polynomials are also usually in or closely around the uncertainty region to best support local RSA accuracy over it. It was found that writing the polynomial RSA in terms of the relatively small local displacements $\vec{w}=[\Delta d, \Delta f, \Delta t]^T$ of the construction points relative to $\vec{z}^o$ yielded much better conditioning of the simultaneous linear and nonlinear equations to be solved for the coefficients of the polynomial functions. Thus. the coordinate transformation in Eqns. A and B was necessary. This allowed significantly more accurate solutions for the coefficients, and therefore more accurate RSAs, than if they were written in terms of the original global parameter coordinates d, f, t.

Hence, we write the linear polynomial RSA $\tilde{r}$ for a generic response quantity r in this subsection in terms of the three local displacement variables $w1$, $w2$, and $w3$:

$$\tilde{r}(\vec{w}) = \mathrm{b0} + \mathrm{b1}\cdot w1 + \mathrm{b2}\cdot w2 + \mathrm{b3}\cdot w3. \qquad (3)$$

To determine the N+1 = 4 coefficients of this 3D linear polynomial (N= the number of dimensions = 3) we need the physics model results at four construction points in the parameter space. The polynomial exactly goes through all four of them by construction. For convenience in solving for the coefficients, one point is placed at the origin location $\vec{z}^o$ of the local coordinate system. Evaluating the physics model at the nominal inputs in [1] corresponding to $\vec{z}^o = \vec{1}$ yields for the TP failure criterion:

$$r(\vec{z} = \vec{z}^o = \vec{1}) = 974.939 \text{ psi}. \qquad (4)$$

Setting this value equal to the RSA value at this point, where Eqn. 3 is written at the coordinates $\vec{w}=\vec{0}$ for the point's location in the local RSA coordinate system, yields

$$\tilde{r}(\vec{w}=\vec{0}) = 974.939 \text{ psi} = \mathrm{b0} + \mathrm{b1}\cdot(w1=0) + \mathrm{b2}\cdot(w2=0) + \mathrm{b3}\cdot(w3=0) = \mathrm{b0}. \qquad (5)$$

The matrix form of the right side of this equation is written in Table 3-1 as an inner product of the elements (1 0 0 0) in the table's row labeled 1 and the column vector of coefficients $\vec{b}$ in the table. The highlighted value in the same row and in the column with heading 'True Y' is the physics model result 974.939 in equations 4 and 5.

The table's labeled row 2 is formed by evaluating the physics model with weld depth $d = 0.026$ *in* while holding all other inputs at nominal. A failure pressure of 910.302 *psi* was obtained with the TP failure criteria. Weld depth values $d = 0.026$ *in* and $d^o = 0.03$ *in* (the nominal value for $\vec{z}^o$) were judged to span enough of the range of weld depths, [0.023 – 0.31] *in*, to yield a representative linear trend of failure pressure versus weld depth. Depth $d = 0.026$ *in* maps to a displacement w1 = -0.004 *in* relative to the nominal value $d^o = 0.03$ *in*. Writing Eqn. 3 for this case yields

$$\tilde{r}(w1 = -0.004,\ w2=0,\ w3=0) = 910.302 \text{ psi} = \text{b0} + \text{b1}\cdot(w1 = -0.004) + \text{b2}\cdot(w2=0) + \text{b3}\cdot(w3=0).$$

The matrix form of this equation is in Table 3-1 as an inner product of the elements (1 -0.004 0 0) in the table's row labeled 2 and the coefficient vector $\vec{b}$, with the physics model result 910.302 *psi* shown highlighted in blue in the same row.

A similar process yields the matrix form of the equation in the table's row labeled 3. For this equation, the physics model with perfect heat transfer across the vertical and horizontal sections of the gap between the can lid and wall in Figure 2 (full thermal-contact effect fraction $f = 1$) was run with all the other inputs $\vec{z}^o$. A failure pressure of 893.482 *psi* is obtained for the TP criterion. This yielded an opposite extreme to the nominal result in Eqn. 4 using the physics model with no heat transfer in the gap region (thermal-contact effect fraction $f = 0$). The thermal-contact effect fraction $f = 1$ relative to the nominal value $f = 0$ maps to the perturbation term $w2 = +1$ highlighted in yellow in the table's row labeled 3.

A similar process yields the matrix form of the equation in the table's row labeled 4. For this equation the physics model was evaluated with wall thickness $t = 0.062$ *in* while holding all other inputs at nominal. A failure pressure of 957.303 *psi* was obtained for the TP failure criterion. This thickness lies at the lower extreme versus the nominal thickness 0.0645 *in* which lies at the upper extreme of the uncertainty range. Wall thickness $t = 0.062$ *in* relative to the nominal value $t = 0.0645$ *in* maps to a perturbation term $w3 = -0.0025$ *in* highlighted in yellow in the table's row labeled 4.

The four simultaneous linear equations in matrix form in Table 3-1are solved in a Microsoft XL spreadsheet as follows. Four initial values are posed for the 'coeffs. {b}' column in the table and then the optimization based nonlinear solver is employed to iterate on the values until the matrix-vector products in column 'A*b = y_predicted' match the 'True Y' values from the physics model runs to within negligibly small differences whose squared values are listed in the 'Diff. Squared' column. A nonlinear solver is used because that is all that is available in XL, but a direct solve could easily be performed on the set of linear equations. When quadratic terms are added to the polynomial RSAs (later in this subsection), corresponding nonlinear equations exist in the set of equations to be solved, so an iterative solver must be used.

Table 3-1. Equation sets and solved coefficients for <u>linear</u> polynomial response surfaces for TP and EQPS failure pressures as a function of the <u>aleatory</u> model parameters.

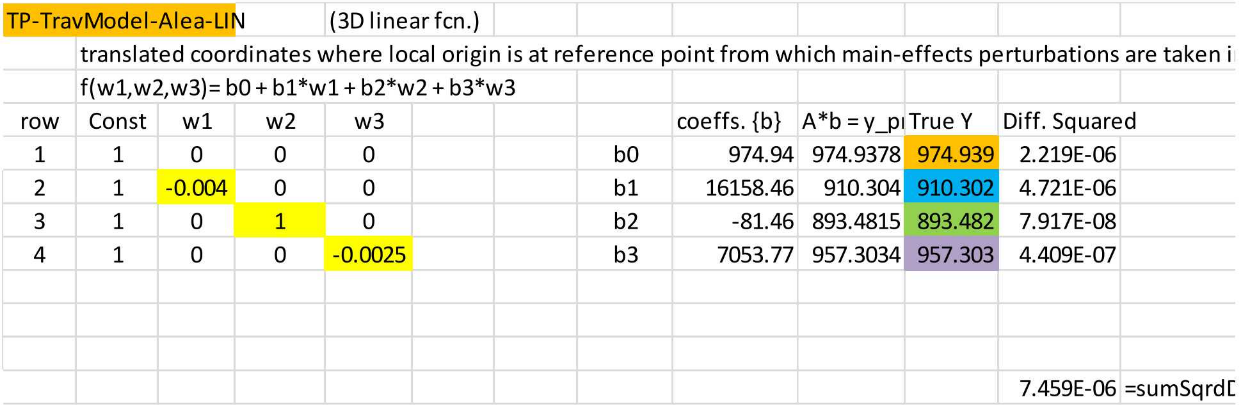

TP-TravModel-Alea-LIN (3D linear fcn.)

translated coordinates where local origin is at reference point from which main-effects perturbations are taken i

f(w1,w2,w3)= b0 + b1*w1 + b2*w2 + b3*w3

row	Const	w1	w2	w3				coeffs. {b}	A*b = y_p	True Y	Diff. Squared	
1	1	0	0	0			b0	974.94	974.9378	974.939	2.219E-06	
2	1	-0.004	0	0			b1	16158.46	910.304	910.302	4.721E-06	
3	1	0	1	0			b2	-81.46	893.4815	893.482	7.917E-08	
4	1	0	0	-0.0025			b3	7053.77	957.3034	957.303	4.409E-07	
											7.459E-06	=sumSqrd

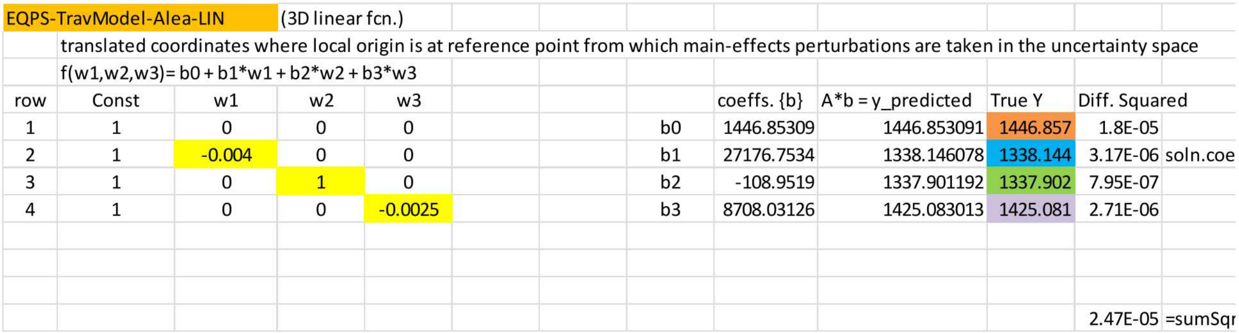

EQPS-TravModel-Alea-LIN (3D linear fcn.)

translated coordinates where local origin is at reference point from which main-effects perturbations are taken in the uncertainty space

f(w1,w2,w3)= b0 + b1*w1 + b2*w2 + b3*w3

row	Const	w1	w2	w3				coeffs. {b}	A*b = y_predicted	True Y	Diff. Squared	
1	1	0	0	0			b0	1446.85309	1446.853091	1446.857	1.8E-05	
2	1	-0.004	0	0			b1	27176.7534	1338.146078	1338.144	3.17E-06	soln.coe
3	1	0	1	0			b2	-108.9519	1337.901192	1337.902	7.95E-07	
4	1	0	0	-0.0025			b3	8708.03126	1425.083013	1425.081	2.71E-06	
											2.47E-05	=sumSqr

Monte Carlo Sampling of Model Input Uncertainties and Propagation through Linear RSAs

The linear RSA Eqn. 3 can be evaluated for model input parameter deviations (w1, w2, and w3) from the nominal inputs $\vec{z}^{o}$. The relevant uncertainty ranges for parameter deviations are listed in the green colored cells in Table 3-2. These ranges map to the ranges of the untransformed parameter uncertainties listed in bullets near the beginning of this section. Below the green heading cells in columns C - E of Table 3-2 are ten thousand (10k) random Monte Carlo (MC) samples of each variable w_i sampled uniformly over its range. The summary statistics at the bottom of the table show that the maximum, minimum, mean, and standard deviation of the samples in each column do not change significantly when increasing from 5k to 10k samples, so 5k or 10k samples are deemed sufficient for the analysis purposes described next.

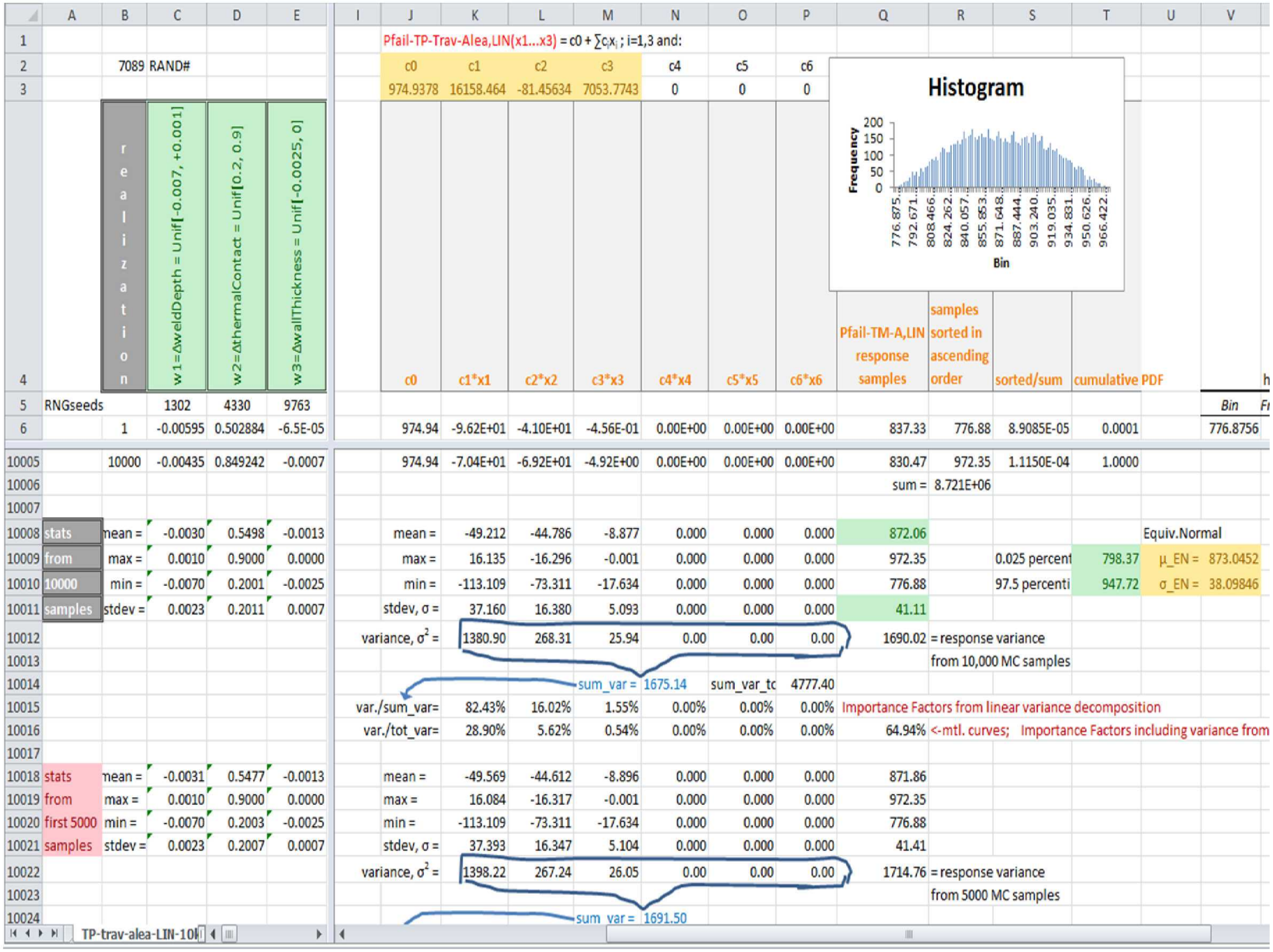

	A	B	C	D	E	I	J	K	L	M	N	O	P	Q	R	S	T	U	V	W
1							Pfail-TP-Trav-Alea,LIN(x1...x3) = c0 + $\sum c_i x_i$; i=1,3 and:													
2		7089	RAND#				c0	c1	c2	c3	c4	c5	c6							
3							974.9378	16158.464	-81.45634	7053.7743	0	0	0							
4		realization	w1=ΔweldDepth = Unif[-0.007, +0.001]	w2=ΔthermalContact = Unif[0.2, 0.9]	w3=ΔwallThickness = Unif[-0.0025, 0]		c0	c1*x1	c2*x2	c3*x3	c4*x4	c5*x5	c6*x6	Pfail-TM-A,LIN response samples	samples sorted in ascending order	sorted/sum	cumulative PDF			h
5	RNGseeds		1302	4330	9763														*Bin*	*F*
6		1	-0.00595	0.502884	-6.5E-05		974.94	-9.62E+01	-4.10E+01	-4.56E-01	0.00E+00	0.00E+00	0.00E+00	837.33	776.88	8.9085E-05	0.0001		776.8756	
10005		10000	-0.00435	0.849242	-0.0007		974.94	-7.04E+01	-6.92E+01	-4.92E+00	0.00E+00	0.00E+00	0.00E+00	830.47	972.35	1.1150E-04	1.0000			
10006														sum =	8.721E+06					
10007																				
10008	stats	mean =	-0.0030	0.5498	-0.0013		mean =	-49.212	-44.786	-8.877	0.000	0.000	0.000	872.06				Equiv.Normal		
10009	from	max =	0.0010	0.9000	0.0000		max =	16.135	-16.296	-0.001	0.000	0.000	0.000	972.35		0.025 percent	798.37	μ_EN =	873.0452	
10010	10000	min =	-0.0070	0.2001	-0.0025		min =	-113.109	-73.311	-17.634	0.000	0.000	0.000	776.88		97.5 percenti	947.72	σ_EN =	38.09846	
10011	samples	stdev =	0.0023	0.2011	0.0007		stdev, σ =	37.160	16.380	5.093	0.000	0.000	0.000	41.11						
10012							variance, σ^2 =	1380.90	268.31	25.94	0.00	0.00	0.00	1690.02	= response variance					
10013															from 10,000 MC samples					
10014										sum_var =	1675.14	sum_var_tc	4777.40							
10015							var./sum_var=	82.43%	16.02%	1.55%	0.00%	0.00%	0.00%	Importance Factors from linear variance decomposition						
10016							var./tot_var=	28.90%	5.62%	0.54%	0.00%	0.00%	0.00%	64.94%	<-mtl. curves; Importance Factors including variance from					
10017																				
10018	stats	mean =	-0.0031	0.5477	-0.0013		mean =	-49.569	-44.612	-8.896	0.000	0.000	0.000	871.86						
10019	from	max =	0.0010	0.9000	0.0000		max =	16.084	-16.317	-0.001	0.000	0.000	0.000	972.35						
10020	first 5000	min =	-0.0070	0.2003	-0.0025		min =	-113.109	-73.311	-17.634	0.000	0.000	0.000	776.88						
10021	samples	stdev =	0.0023	0.2007	0.0007		stdev, σ =	37.393	16.347	5.104	0.000	0.000	0.000	41.41						
10022							variance, σ^2 =	1398.22	267.24	26.05	0.00	0.00	0.00	1714.76	= response variance					
10023															from 5000 MC samples					
10024										sum_var =	1691.50									

Table 3-2. Spreadsheet generation and Linear RSA/TP propagation of MC samples of model input parameter deviations $\vec{w}$ due to the aleatory *parametric* uncertainties listed near beginning of this section.

Propagation of the 10k MC row-sets of the input parameter values in columns C - E through the linear RSA is accomplished in columns J - M of the spreadsheet in Table 3-2. In columns J – M, the polynomial coefficient values in row 3 come from Table 3-1 as the linear polynomial coefficients b0 - b3 for the TP failure criteria. These correspond to the generic coefficients c0 - c3 in row 2 (columns C - E) of the table. These coefficients are part of a generic linear polynomial in up to six variables x_i (which correspond to variables w_i in the present case). Setting coefficients c4=c5=c6=0 in the spreadsheet reduces the potential 6D linear response surface to the desired 3D linear RSA in 3 variables, Eqn. 3.

For a given row in the spreadsheet, the MC realizations of the three random variables w_i in columns C - E are multiplied by coefficients c_i (= b_i) as defined at the bottom of row 4 in columns K - M. These three monomial values and the constant term c0 (= b0) are summed (per Eqn. 3) and the result is put in column Q. Hence, column Q contains 10k random samples of TP failure pressure uncertainty from linearly propagated input aleatory uncertainties. A histogram of the 10k results is shown in the table.

Similar procedures and considerations hold for the EQPS failure criteria results in Table 3-3. The 10k MC row-sets of input parameter values in columns C - E are the same as in Table 3-2. In columns J - M of Table 3-3 the values in row 3 come from Table 3-1 as the linear polynomial coefficients b0 - b3 for the EQPS failure criteria. Column Q of Table 3-3 contains 10k random samples of EQPS failure pressure uncertainty from linearly propagated input aleatory uncertainties. A histogram of the 10k results is plotted in the table.

Uncertainty and Sensitivity Analysis of Linearized Uncertainty Propagation Results

Rows 10,008 – 10,012 in Table 3-3 list various summary statistics (named in column J) for the 10k values in each column K - Q. Each input parameter's uncertainty when linearly mapped into response uncertainty produces a response variance listed in row 10012, columns K - P. In linear uncertainty propagation, the total variance of the output response quantity is equal to the sum of response variances contributed by the individual sources. Row 10,014 lists the sum, 1675 psi^2, in blue print. The square root of this gives a standard deviation of 41 *psi*.

As a check, this sum of variances, 1675 psi^2, is within 0.9% of the variance 1690 psi^2 in row/column 10012/Q computed directly from the 10k response samples in column Q. The 5k-sample sum of variances 1692 psi^2 in row/column 10024/N is about 1.3% different from the 5k-sample variance of 1715 psi^2 in row/column 10022/Q. Thus, the difference between sum of variances and the direct sample variance from column Q is somewhat larger using 5k samples than with 10k samples. Nonetheless, the 5k and 10k sample variances in column Q are within 1.5% of each other and the sums of variances in column N are within 1% of each other for 5k and 10k samples. This suggests that sampling convergence error is small compared to other errors and uncertainties in the validation UQ analysis to follow. Accordingly, sample sizes of 10k are used for all final results in what follows.

The fractional contribution of each uncertainty source to the summed response variance is listed in row 10,015. Columns K, L, M of this row reveal that weld depth uncertainty is responsible for about 82% of the summed response variance, thermal-contact fraction is responsible for about 16%, and wall thickness is only responsible for 2%. (The sensitivity fractions listed in row 10,016 also involve variance contributed by material stress-strain curve variability as determined in Section 4 .)

Table 3-3. Spreadsheet generation and Linear RSA/EQPS propagation of MC samples of model input parameter deviations $\vec{w}$ due to the aleatory *parametric* uncertainties listed near beginning of this section.

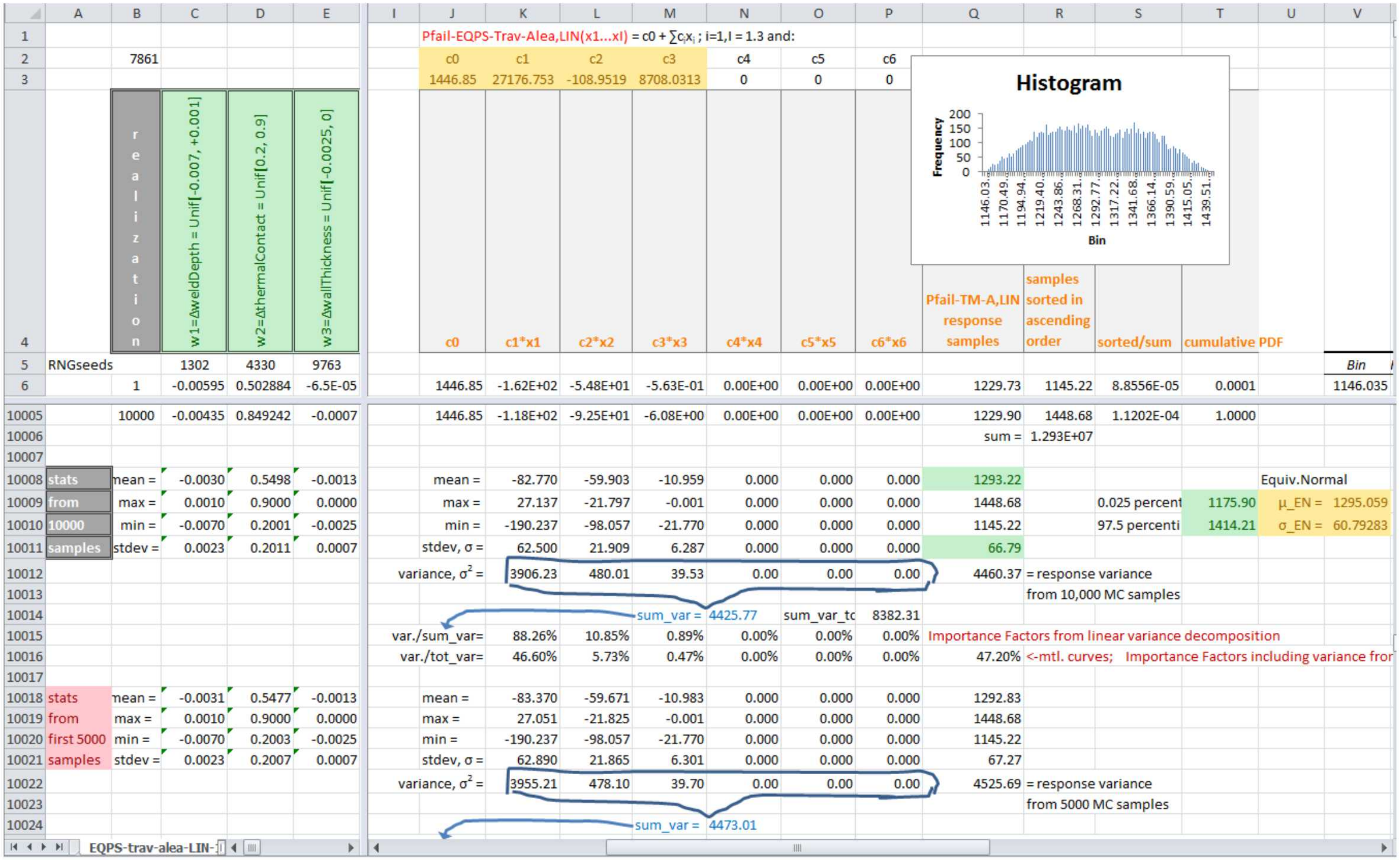

	A	B	C	D	E	I	J	K	L	M	N	O	P	Q	R	S	T	U	V
1							Pfail-EQPS-Trav-Alea,LIN(x1...xI) = c0 + $\sum c_i x_i$; i=1,I = 1.3 and:												
2		7861					c0	c1	c2	c3	c4	c5	c6						
3							1446.85	27176.753	-108.9519	8708.0313	0	0	0						
4		realization	w1=ΔweldDepth = Unif[-0.007, +0.001]	w2=ΔthermalContact = Unif[0.2, 0.9]	w3=ΔwallThickness = Unif[-0.0025, 0]		c0	c1*x1	c2*x2	c3*x3	c4*x4	c5*x5	c6*x6	Pfail-TM-A,LIN response samples	samples sorted in ascending order	sorted/sum	cumulative PDF		
5	RNGseeds		1302	4330	9763														*Bin*
6		1	-0.00595	0.502884	-6.5E-05		1446.85	-1.62E+02	-5.48E+01	-5.63E-01	0.00E+00	0.00E+00	0.00E+00	1229.73	1145.22	8.8556E-05	0.0001		1146.035
10005		10000	-0.00435	0.849242	-0.0007		1446.85	-1.18E+02	-9.25E+01	-6.08E+00	0.00E+00	0.00E+00	0.00E+00	1229.90	1448.68	1.1202E-04	1.0000		
10006														sum =	1.293E+07				
10007																			
10008	stats	mean =	-0.0030	0.5498	-0.0013		mean =	-82.770	-59.903	-10.959	0.000	0.000	0.000	1293.22				Equiv.Normal	
10009	from	max =	0.0010	0.9000	0.0000		max =	27.137	-21.797	-0.001	0.000	0.000	0.000	1448.68		0.025 percent	1175.90	μ_EN =	1295.059
10010	10000	min =	-0.0070	0.2001	-0.0025		min =	-190.237	-98.057	-21.770	0.000	0.000	0.000	1145.22		97.5 percenti	1414.21	σ_EN =	60.79283
10011	samples	stdev =	0.0023	0.2011	0.0007		stdev, σ =	62.500	21.909	6.287	0.000	0.000	0.000	66.79					
10012							variance, σ^2 =	3906.23	480.01	39.53	0.00	0.00	0.00	4460.37	= response variance				
10013															from 10,000 MC samples				
10014										sum_var =	4425.77	sum_var_tc	8382.31						
10015							var./sum_var=	88.26%	10.85%	0.89%	0.00%	0.00%	0.00%	Importance Factors from linear variance decomposition					
10016							var./tot_var=	46.60%	5.73%	0.47%	0.00%	0.00%	0.00%	47.20%	<-mtl. curves; Importance Factors including variance fror				
10017																			
10018	stats	mean =	-0.0031	0.5477	-0.0013		mean =	-83.370	-59.671	-10.983	0.000	0.000	0.000	1292.83					
10019	from	max =	0.0010	0.9000	0.0000		max =	27.051	-21.825	-0.001	0.000	0.000	0.000	1448.68					
10020	first 5000	min =	-0.0070	0.2003	-0.0025		min =	-190.237	-98.057	-21.770	0.000	0.000	0.000	1145.22					
10021	samples	stdev =	0.0023	0.2007	0.0007		stdev, σ =	62.890	21.865	6.301	0.000	0.000	0.000	67.27					
10022							variance, σ^2 =	3955.21	478.10	39.70	0.00	0.00	0.00	4525.69	= response variance				
10023															from 5000 MC samples				
10024										sum_var =	4473.01								

Similar procedures and considerations hold for the EQPS failure criteria results in Table 3-3. The linearized response variances are given in row 10,012. Row 10,014 lists in blue letters the sum of the variances in row 10,012. This sum is 4426 *psi*^{2}. The square root of this gives a standard deviation of 67 *psi*. This is about 63% higher than the 41 *psi* standard deviation predicted with the TP failure criteria. Thus, considerably larger failure pressure variability is predicted with the EQPS failure criteria than with the TP criteria.

As a check, the sum of variances, 4426, in Table 3-3 is within 0.7% of the variance result 4460 in row/column 10012/Q computed directly from the 10k response samples in column Q. The 5k-sample sum of variances 4473 in row/column 10024/N is about 1.2% different from the 5k-sample variance of 4526 in row/column 10022/Q. Again, as with the TP failure criteria, the difference between sum of variances and the direct sample variance from column Q is somewhat larger using 5k samples than with 10k samples. Nonetheless, the 5k and 10k sample variances in column Q are within 1.5% of each other and the sums of variances in column N are within 1.1% of each other for 5k and 10k samples. Again, the 10k samples appear adequate relative to other errors and uncertainties in the validation UQ analysis.

Columns K, L, M of row 10,015 indicate that weld depth uncertainty is responsible for about 88.2% of the summed response variance, thermal-contact fraction is responsible for about 10.9%, and wall thickness is only responsible for 0.9%. This split of response sensitivity to these input uncertainty sources is not substantially different than with the TP failure criteria. In subsection 12.4.1.3, we discuss the sensitivity fractions listed in row 10,016.

Construction of 3D Linear-Quadratic Response Surface Approximation

From the linear sensitivity analysis, weld depth and lid thermal contact uncertainties are both substantial contributors to total response uncertainty. Therefore, it is desirable to see if response nonlinearities to these factors significantly impact the uncertainty results.

We first consider weld depth. Because this was found to be such a dominant factor, two new models with weld depths of 0.024 *in* and 0.028 *in* were run at nominal conditions for all other factors. Figure 5 shows the results for all four weld depths analyzed, 0.024 *in*, 0.026 *in*, 0.028 *in*, and 0.03 *in*. Among the two new results at 0.024 *in* and 0.028 *in*, 0.024 *in* was chosen for the following quadratic response analysis because it lies nearest to the lower bound (0.023 *in*) of the weld depth's uncertainty range, where failure pressure is lowest and breach occurs earliest, and as such, poses the biggest threat to safety margins on container failure.

Working with the new 0.024 *in* weld depth and the previous two depths 0.026 and 0.03 *in*, enables upgrading to a quadratic approximation of response variation in this factor. The associated linear+quadratic polynomial equation is presented in Table 3-4. The new equation has the quadratic term in red, b1-1*w1*w1, added to the linear terms from Eqn. 3. Now the five coefficients b0 - b1 and b1-1 must be solved for. To do this, the new linear+quadratic polynomial equation is evaluated at the five input parameter sets (five construction points in the parameter space) where physics model results exist—the polynomial exactly goes through all five points. These are the four previous construction points from the linear development + the new physics model result at 0.024 *in* weld depth.

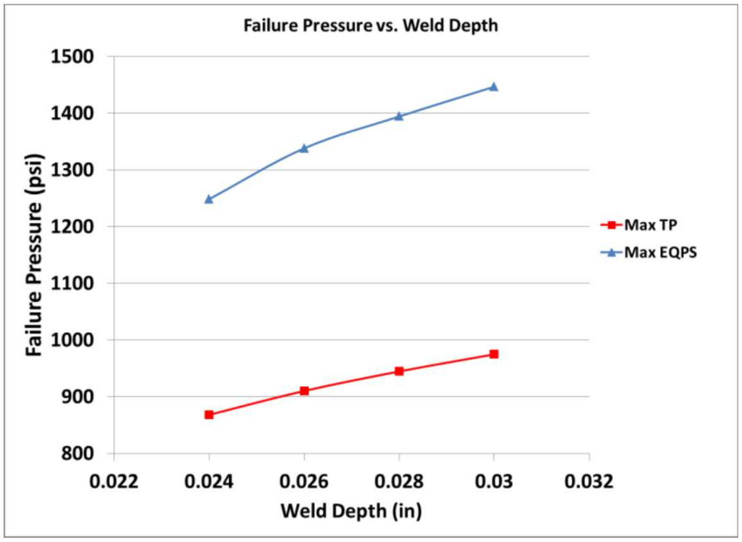

Figure 5. Failure pressure predictions from critical TP and EQPS values for four weld depths 0.024, 0.026, 0.028, and 0.03 in. and all other inputs at nominal values. (Figure from [7].)

Table 3-4. Equation sets and solved coefficients for <u>linear+quadratic</u> polynomial response surfaces for CompSim model TP and EQPS failure pressures as a function of the <u>aleatory</u> model parameters

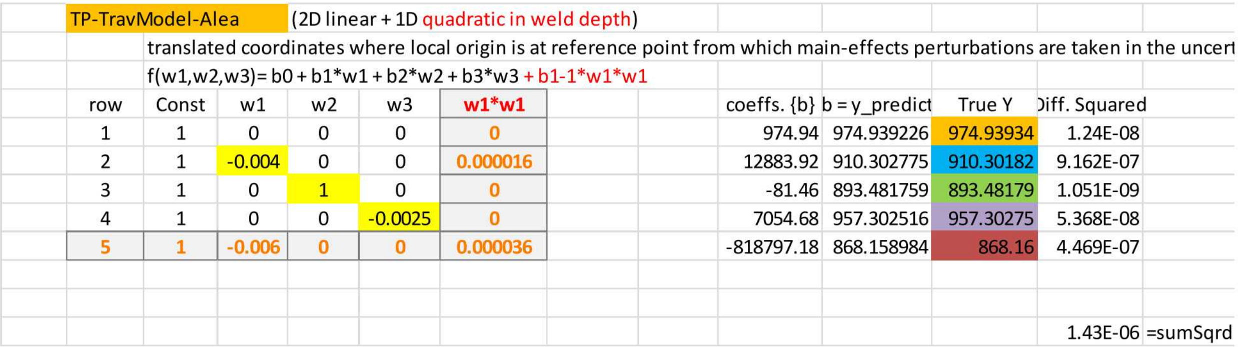

TP-TravModel-Alea (2D linear + 1D quadratic in weld depth)

translated coordinates where local origin is at reference point from which main-effects perturbations are taken in the uncert

f(w1,w2,w3)= b0 + b1*w1 + b2*w2 + b3*w3 + b1-1*w1*w1

row	Const	w1	w2	w3	w1*w1	coeffs. {b}	b = y_predict	True Y	Diff. Squared	
1	1	0	0	0	0	974.94	974.939226	974.93934	1.24E-08	
2	1	-0.004	0	0	0.000016	12883.92	910.302775	910.30182	9.162E-07	
3	1	0	1	0	0	-81.46	893.481759	893.48179	1.051E-09	
4	1	0	0	-0.0025	0	7054.68	957.302516	957.30275	5.368E-08	
5	1	-0.006	0	0	0.000036	-818797.18	868.158984	868.16	4.469E-07	
									1.43E-06	=sumSqrd

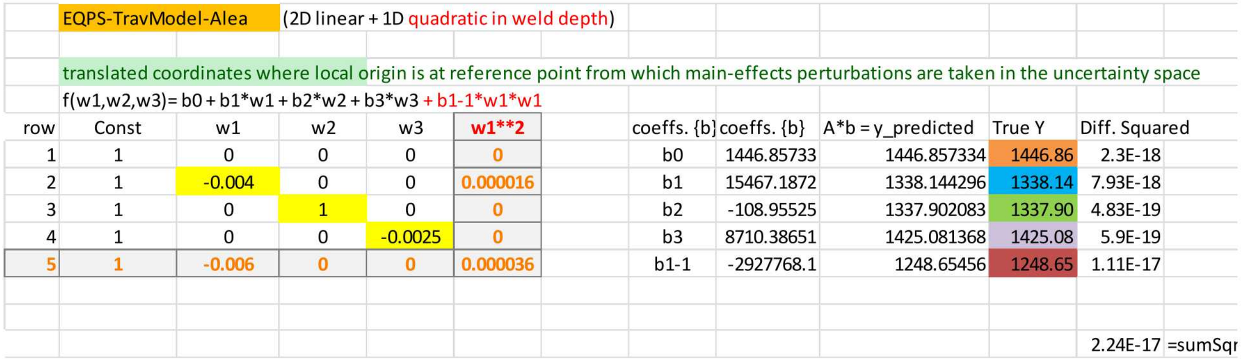

EQPS-TravModel-Alea (2D linear + 1D quadratic in weld depth)

translated coordinates where local origin is at reference point from which main-effects perturbations are taken in the uncertainty space

f(w1,w2,w3)= b0 + b1*w1 + b2*w2 + b3*w3 + b1-1*w1*w1

row	Const	w1	w2	w3	w1**2	coeffs. {b}	coeffs. {b}	A*b = y_predicted	True Y	Diff. Squared	
1	1	0	0	0	0	b0	1446.85733	1446.857334	1446.86	2.3E-18	
2	1	-0.004	0	0	0.000016	b1	15467.1872	1338.144296	1338.14	7.93E-18	
3	1	0	1	0	0	b2	-108.95525	1337.902083	1337.90	4.83E-19	
4	1	0	0	-0.0025	0	b3	8710.38651	1425.081368	1425.08	5.9E-19	
5	1	-0.006	0	0	0.000036	b1-1	-2927768.1	1248.65456	1248.65	1.11E-17	
										2.24E-17	=sumSqr

Table 3-5 presents the matrix form of the five new equations in five unknowns. Note that the solved value of coefficient b1 changes from the value in the linear equations in Table 3-1, but the solved values of coefficients b0, b2, and b3 do not change. This is because the equations for these latter coefficients, rows labeled 1, 3, and 4 do not change from Table 3-1 to Table 3-5. But row 2's equation changes from Table 3-1 to Table 3-5. The equations in row 2 and the new row 5 both involve non-zero terms multiplying coefficients b1 and b1-1 pertaining to the weld-depth variable and the quadratic function in this variable.

Next we consider the lid-wall thermal-contact effect. The uncertainty in the thermal-contact fraction *f* variable has a substantial (19%) contribution to the summed response variance from the three factors in this section. Normally, this large of a relative contribution would warrant an upgrade to a quadratic response approximation in this variable, but this was precluded in the present study. It is clear that bounding treatments for lid thermal contact with the can wall are the no-contact and full perfect contact extremes described earlier. However, it is unclear what a given intermediate heat transfer condition would correspond to in terms of % thermal-contact effect, or vice-versa, e.g. what a 50% thermal-contact effect fraction would correspond to in terms of heat-transfer conditions between the lid and can wall. Although physics model calculations of intermediate cases of air radiative heat transfer across the gap between the lid and can wall were used to roughly estimate a physically guided lower bound of 20% thermal-contact effect fraction as described in section 12.3, the 20% value was not judged precise enough to pair with these heat transfer conditions to build an accurate quadratic variation function in this factor. Therefore, we elected to stay with the linear representation in this factor for the uncertainty propagation to be discussed next. Examples of linear-quadratic response surface construction for multiple variables treated quadratically can be found in [10], [11].

MC Propagation of Model Input Uncertainties through Linear-Quadratic RSA

As explained above, the equations and coefficient solutions in Table 3-4 comprise the TP linear+quadratic RSA to be used for the uncertainty propagation discussed next. The relevant uncertainty ranges and MC samples of parameter deviations in columns C - E of Table 3-5 are the same as in columns C - E of Table 3-2. Propagation of the 10k MC row-sets of the input parameter values in columns C - E through the linear+quadratic RSA function is accomplished in columns J - N of the spreadsheet in Table 3-5. In these columns, the values in row 3 come from the Table 3-4 polynomial coefficients {b} for the TP failure criteria. Column Q in Table 3-5 contains 10k random samples of linear-quadratic RSA failure pressure uncertainty for TP failure criteria. A histogram of the 10k results is shown in the table.

Similar procedures and considerations hold for the EQPS failure criteria results in Table 3-6. The 10k MC row-sets of input parameter values in columns C - E are the same as in Table 3-3 and Table 3-2. In columns J - N of Table 3-6, the values in row 3 come from the Table 3-4 polynomial coefficients {b} for the EQPS failure criteria. Column Q in Table 3-6 contains 10k random samples of linear-quadratic RSA response uncertainty for EQPS failure pressure. A histogram of the 10k results is plotted in the table.

Table 3-5. Generation and Linear+Quadratic RSA/TP propagation of MC samples of model input parameter deviations $\vec{w}$ due to the aleatory *parametric* uncertainties.

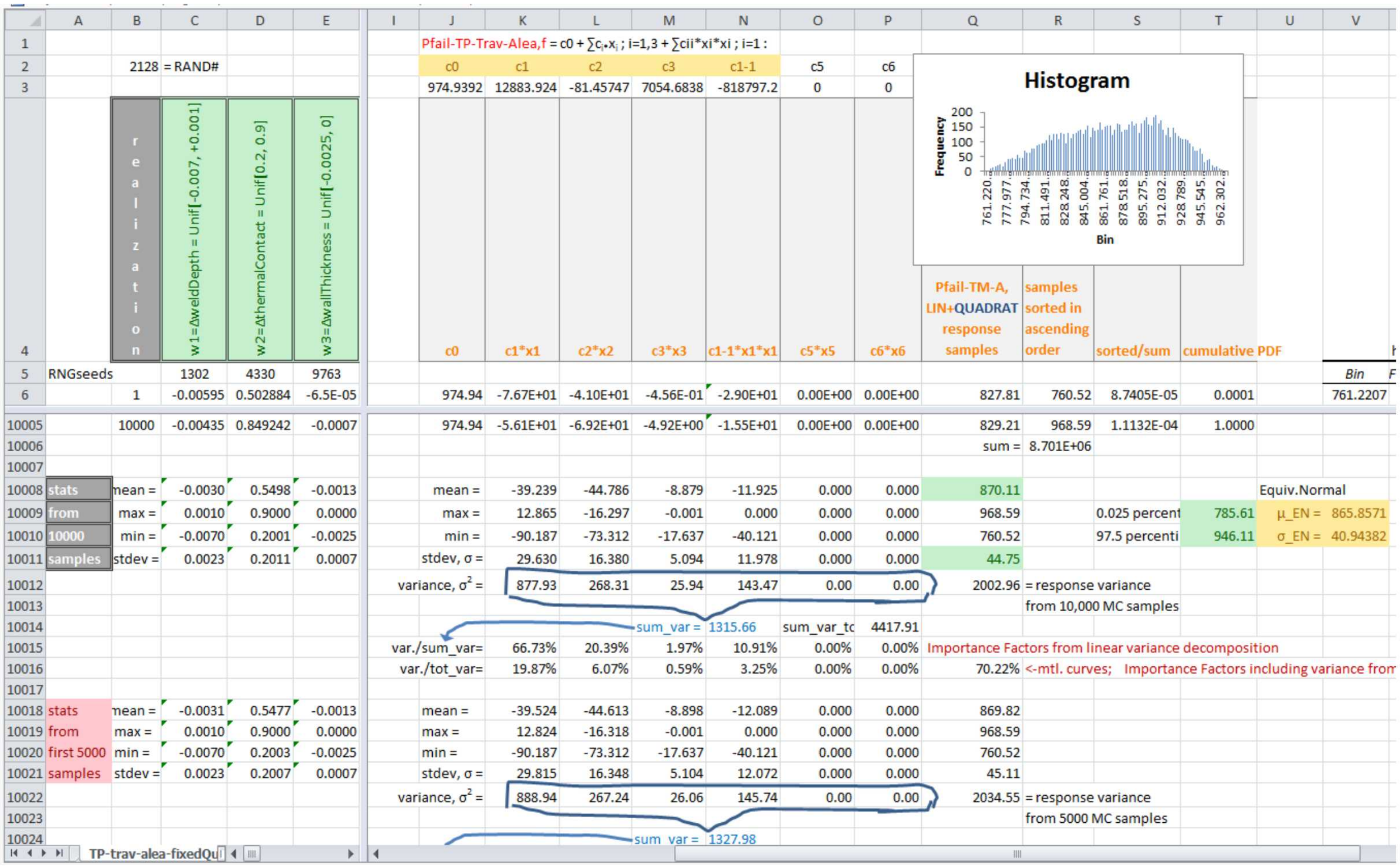

	A	B	C	D	E	I	J	K	L	M	N	O	P	Q	R	S	T	U	V
1							Pfail-TP-Trav-Alea,f = c0 + $\sum c_i \cdot x_i$; i=1,3 + ∑cii*xi*xi ; i=1 :												
2		2128	= RAND#				c0	c1	c2	c3	c1-1	c5	c6						
3							974.9392	12883.924	-81.45747	7054.6838	-818797.2	0	0						
4		realization	w1=ΔweldDepth = Unif[-0.007, +0.001]	w2=ΔthermalContact = Unif[0.2, 0.9]	w3=ΔwallThickness = Unif[-0.0025, 0]		c0	c1*x1	c2*x2	c3*x3	c1-1*x1*x1	c5*x5	c6*x6	Pfail-TM-A, LIN+QUADRAT response samples	samples sorted in ascending order	sorted/sum	cumulative	PDF	
5	RNGseeds		1302	4330	9763														*Bin*
6		1	-0.00595	0.502884	-6.5E-05		974.94	-7.67E+01	-4.10E+01	-4.56E-01	-2.90E+01	0.00E+00	0.00E+00	827.81	760.52	8.7405E-05	0.0001		761.2207
10005		10000	-0.00435	0.849242	-0.0007		974.94	-5.61E+01	-6.92E+01	-4.92E+00	-1.55E+01	0.00E+00	0.00E+00	829.21	968.59	1.1132E-04	1.0000		
10006														sum =	8.701E+06				
10007																			
10008	stats	mean =	-0.0030	0.5498	-0.0013		mean =	-39.239	-44.786	-8.879	-11.925	0.000	0.000	870.11				Equiv.Normal	
10009	from	max =	0.0010	0.9000	0.0000		max =	12.865	-16.297	-0.001	0.000	0.000	0.000	968.59		0.025 percent	785.61	μ_EN =	865.8571
10010	10000	min =	-0.0070	0.2001	-0.0025		min =	-90.187	-73.312	-17.637	-40.121	0.000	0.000	760.52		97.5 percenti	946.11	σ_EN =	40.94382
10011	samples	stdev =	0.0023	0.2011	0.0007		stdev, σ =	29.630	16.380	5.094	11.978	0.000	0.000	44.75					
10012							variance, σ^2 =	877.93	268.31	25.94	143.47	0.00	0.00	2002.96	= response variance				
10013															from 10,000 MC samples				
10014										sum_var =	1315.66	sum_var_tc	4417.91						
10015							var./sum_var=	66.73%	20.39%	1.97%	10.91%	0.00%	0.00%	Importance Factors from linear variance decomposition					
10016							var./tot_var=	19.87%	6.07%	0.59%	3.25%	0.00%	0.00%	70.22%	<-mtl. curves; Importance Factors including variance from				
10017																			
10018	stats	mean =	-0.0031	0.5477	-0.0013		mean =	-39.524	-44.613	-8.898	-12.089	0.000	0.000	869.82					
10019	from	max =	0.0010	0.9000	0.0000		max =	12.824	-16.318	-0.001	0.000	0.000	0.000	968.59					
10020	first 5000	min =	-0.0070	0.2003	-0.0025		min =	-90.187	-73.312	-17.637	-40.121	0.000	0.000	760.52					
10021	samples	stdev =	0.0023	0.2007	0.0007		stdev, σ =	29.815	16.348	5.104	12.072	0.000	0.000	45.11					
10022							variance, σ^2 =	888.94	267.24	26.06	145.74	0.00	0.00	2034.55	= response variance				
10023															from 5000 MC samples				
10024										sum_var =	1327.98								

TP-trav-alea-fixedQu

Table 3-6. Generation and Linear+Quadratic RSA/EQPS propagation of Monte Carlo samples of model input parameter deviations $\vec{w}$ due to the aleatory *parametric* uncertainties.

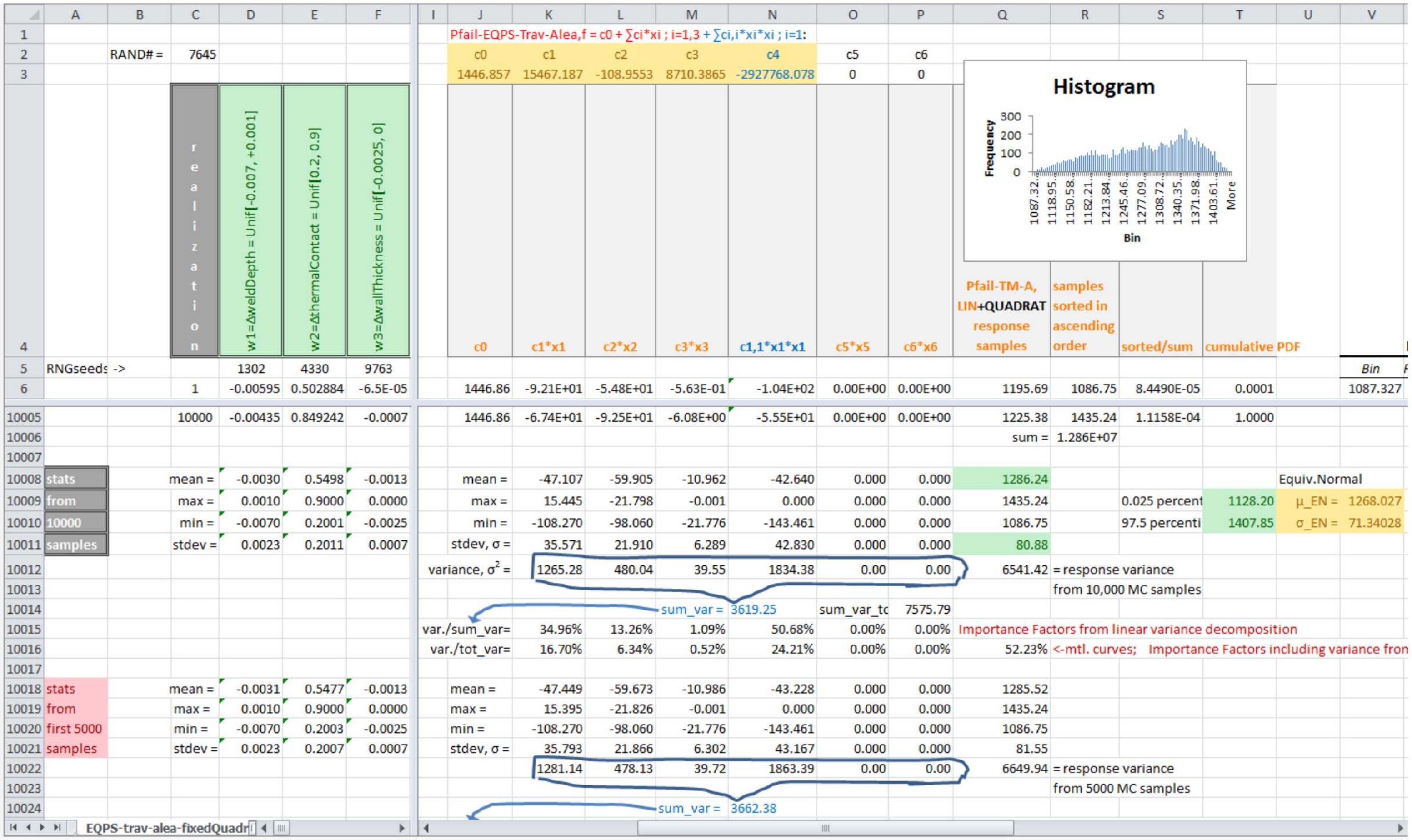

	A	B	C	D	E	F	I	J	K	L	M	N	O	P	Q	R	S	T	U	V
1								Pfail-EQPS-Trav-Alea,f = c0 + ∑ci*xi ; i=1,3 + ∑ci,i*xi*xi ; i=1:												
2		RAND# =	7645					c0	c1	c2	c3	c4	c5	c6						
3								1446.857	15467.187	-108.9553	8710.3865	-2927768.078	0	0						
4			realization	w1=ΔweldDepth = Unif[-0.007, +0.001]	w2=ΔthermalContact = Unif[0.2, 0.9]	w3=ΔwallThickness = Unif[-0.0025, 0]		c0	c1*x1	c2*x2	c3*x3	c1,1*x1*x1	c5*x5	c6*x6	Pfail-TM-A, LIN+QUADRAT response samples	samples sorted in ascending order	sorted/sum	cumulative PDF		
5	RNGseeds ->			1302	4330	9763														Bin
6			1	-0.00595	0.502884	-6.5E-05		1446.86	-9.21E+01	-5.48E+01	-5.63E-01	-1.04E+02	0.00E+00	0.00E+00	1195.69	1086.75	8.4490E-05	0.0001		1087.327
10005			10000	-0.00435	0.849242	-0.0007		1446.86	-6.74E+01	-9.25E+01	-6.08E+00	-5.55E+01	0.00E+00	0.00E+00	1225.38	1435.24	1.1158E-04	1.0000		
10006															sum =	1.286E+07				
10007																				
10008	stats		mean =	-0.0030	0.5498	-0.0013		mean =	-47.107	-59.905	-10.962	-42.640	0.000	0.000	1286.24				Equiv.Normal	
10009	from		max =	0.0010	0.9000	0.0000		max =	15.445	-21.798	-0.001	0.000	0.000	0.000	1435.24		0.025 percent	1128.20	μ_EN =	1268.027
10010	10000		min =	-0.0070	0.2001	-0.0025		min =	-108.270	-98.060	-21.776	-143.461	0.000	0.000	1086.75		97.5 percenti	1407.85	σ_EN =	71.34028
10011	samples		stdev =	0.0023	0.2011	0.0007		stdev, σ =	35.571	21.910	6.289	42.830	0.000	0.000	80.88					
10012								variance, σ^2 =	1265.28	480.04	39.55	1834.38	0.00	0.00	6541.42	= response variance				
10013																from 10,000 MC samples				
10014											sum_var =	3619.25	sum_var_tc	7575.79						
10015								var./sum_var=	34.96%	13.26%	1.09%	50.68%	0.00%	0.00%	Importance Factors from linear variance decomposition					
10016								var./tot_var=	16.70%	6.34%	0.52%	24.21%	0.00%	0.00%	52.23%	<-mtl. curves; Importance Factors including variance fron				
10017																				
10018	stats		mean =	-0.0031	0.5477	-0.0013		mean =	-47.449	-59.673	-10.986	-43.228	0.000	0.000	1285.52					
10019	from		max =	0.0010	0.9000	0.0000		max =	15.395	-21.826	-0.001	0.000	0.000	0.000	1435.24					
10020	first 5000		min =	-0.0070	0.2003	-0.0025		min =	-108.270	-98.060	-21.776	-143.461	0.000	0.000	1086.75					
10021	samples		stdev =	0.0023	0.2007	0.0007		stdev, σ =	35.793	21.866	6.302	43.167	0.000	0.000	81.55					
10022									1281.14	478.13	39.72	1863.39	0.00	0.00	6649.94	= response variance				
10023																from 5000 MC samples				
10024											sum_var =	3662.38								

Uncertainty and Sensitivity Analysis of Linear-Quadratic Uncertainty Propagation Results

One prominent change relative to the linear RSA results is that the linear-quadratic RSA results in Table 3-5 and Table 3-6 each show substantial differences between their response variances in columns Q computed from MC sampling compared to their summed variance results in blue print in column N. For the TP failure criteria, the 10k-sample response variance in Table 3-5 is 2003 *psi*^{2} in cell Q10012 while the summed variance in cell N10014 is 35% less, 1316 *psi*^{2}. This reflects that summing the individual factors' propagated variance contributions is only a valid operation when the uncertainties are linearly propagated. Since this is not the case here, only the variance 2003 *psi*^{2} computed from the 10k response samples in column Q is relevant. The 5k-sample version of this variance is 2036 *psi*^{2} in cell Q10022. This is about 1.6% different from the 10k value. Again, this suggests that sampling convergence error is small relative to other errors and uncertainties in the validation UQ analysis.

Analogous results for the EQPS failure criteria have the 10k-sample response variance 6541 *psi*^{2} in Table 3-6 cell Q10012 about 45% greater than the summed variance in cell N10014. The 10k-sample variance 6541 *psi*^{2} is about 1.7% different from the 5k-sample value in cell Q10022, again indicating relatively small sampling convergence error.

The TP failure pressure standard deviation of 45 *psi* here (corresponding to 10k-sample variance 2003 *psi*^{2}) is about 9% larger than the 41 *psi* standard deviation determined with the linear RSA. The EQPS failure pressure standard deviation of 81 *psi* here (corresponding to 10k-sample variance 6541 *psi*^{2}) is about 21% larger than the 67 *psi* standard deviation determined with the linear RSA. Thus, for both the EQPS and TP failure criteria, the nonlinear upgraded RSA indicates considerably higher failure pressure variability than the linear RSA does.

With the nonlinear RSAs the EQPS standard deviation of 81 *psi* is about 1.8X the TP standard deviation of 45 *psi*. With the linear RSAs, the relative difference is somewhat less: the 67 *psi* for EQPS-linear is about 1.6X the 41*psi* for TP-linear.

Judging from the substantial differences produced by the linear and linear-quadratic RSAs, the upgrade to the nonlinear RSA was necessary. The large results changes suggest that results may continue to change appreciably with further higher-order refinements of the RSA. This would normally be explored with further upgrades to the RSA, but in this study, this was not feasible due to time and resource constraints. Nonetheless, a rough estimate of the failure-pressure variability prediction error due to the potentially under-resolved linear-quadratic response surface is pursued in [11].

Although the summed variances in row 10,014 of Table 3-5 and Table 3-6 are not accurate, the linear-quadratic polynomial terms' sensitivity fractions in row 10,015 are interpreted as rough but useful indicators of response sensitivity to the uncertain inputs. For TP in Table 3-5, the variance contributions in row 10,012 columns K and N for weld-depth linear and quadratic polynomial terms are respectively 67% and 11% of the summed variance. The combined weld depth share is 78% of the response variance, thermal-contact fraction is responsible for 20% (column L), and wall thickness share is 2% (column M). These sensitivities are close to what was found in the linear analysis (82%, 16%, and 2%).

For EQPS in Table 3-6, the weld-depth linear and quadratic polynomial terms respectively contribute 35% and 51% of the summed variance. The combined weld depth share is 86% of the response variance, the thermal-contact fraction share is 13%, and wall thickness share is 1%.

These sensitivities are also very close to what was found in the linear analysis (88%, 11%, and 1%).

Note that the contributed variance from the linear term associated with weld depth (column K in row 10,012) differs from the corresponding value in Table 3-3 for the linear-only RSA. But the other factors of thermal-contact fraction and wall thickness (columns L and M in row 10,012) in Table 3-6 retain the same variance contributions as in Table 3-3 for the linear-only RSA. This is because thermal-contact fraction and wall thickness remain linear (unchanged, not upgraded to quadratic) in the linear-quadratic RSA; the polynomial coefficients for these factors are the same in the linear RSA (Table 3-1) and the linear-quadratic RSA (Table 3-4). Similar observations apply for the TP results.

From Figure 5, when the quadratic variation in failure pressure based on weld depths 0.024 *in*, 0.026 *in*, 0.03 *in* is sampled over the uncertainty range [0.023 *in*, 0.031 *in*], the variance in failure pressure results increases compared to sampling from a linear approximation based on the 0.026 *in* and 0.03 *in* weld depths. Hence, the effect of the upgraded polynomial order in weld depth is to increase the total response variance, as reported above. Since the other factors of thermal-contact fraction and wall thickness retain the same linear contributions to variance as the linear RSA, the increase in response variance is due solely to the increased contribution from the weld-depth factor. An accurate sensitivity fraction would reflect this. But for both TP and EQPS, the linear results show a larger fraction of variance attributed to weld depth variations (e.g., 88% for EQPS) than the linear-quadratic results do (86% for EQPS). This is an artifact of the error involved from forming sensitivity fractions for the nonlinear RSA propagation by using a linear-analogue sensitivity approach. The linear analogue approach applied here can provide simple and rough but useful indication of response sensitivities, but important project resource allocation or program decisions may require a more accurate nonlinear sensitivity analysis (SA) method be employed. References [22]-[24] survey and demonstrate more sophisticated and accurate nonlinear SA methods.

4. Discrete Propagation of Material Strength and Failure Variability to Can Breach-Pressure Variability Predictions

The uncertainty sources considered in this section are the aleatory uncertainties that come in ***discrete*** (not parametric) form of multiple slightly varying stress-strain curves and failure criteria representing stochastic material strength variations in the can lid, weld, and wall materials. These curve-to-curve variations and failure criteria when propagated cause predicted variability (and uncertainty thereof) in can response and failure pressure level. The 16 uncertainties not related to material strength and failure variability are all parametric in nature and are held at nominal values listed in [12] for the purposes of the following material-curve propagations and analysis of results.

Sensitivity studies in the current paper and in [11] and [12] of the effects of the more prominent modeling uncertainties regarding thermal, pressurization, and structural phenomena in the PCAP problem reveal that material curve strength variations are among the most significant causes of failure-pressure predicted variability and uncertainty thereof.

4.1 Dealing with Temperature Dependence of the Material Stress-Strain Curves

Dealing with temperature dependence of the material curves adds a significant difficulty to the discrete propagation problem. This is addressed in the following two data processing steps before propagation can be performed in section 4.2. Brief summaries are given here. See [9] for a detailed explanation and application of the steps.

Step I *- Material stress-strain curves strength-to-failure ranking and down-selection*

In this step, the effective strength of the repeat material curves at each of the seven characterization temperatures (e.g., Figure 3) were ranked and then down-selected to three representative curves (high, medium, and low strength) according to predicted failure pressure predictions from the PCAP can simulations. The isothermal mechanical-only simulations used Mesh 4. At most temperatures only three "good" tests/material curves were obtained, but at some temperatures as much as five experimental curves were obtained and considered in the down-selection to three representative curves of high, medium, and low strength as portrayed in Figure 6.

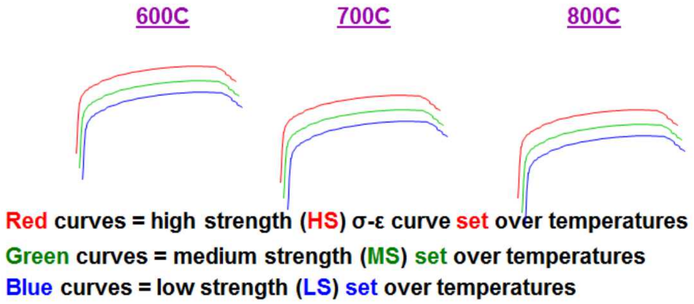

Figure 6. Notional portrayal of high, medium, and low effective strength stress-strain curves at adjacent characterization temperatures.

At a given temperature, the effective strength of each material curve (say for bar stock used in the can lid and base) was determined by the calculated pressure at which <u>weld</u> critical TP or EQPS value was reached (i.e., when can failure was reached). Curve strength rankings were usually the same whether critical weld TP or EQPS value was used. Recall that the weld material was specified to be the same as the wall material because it was weaker than the lid material, so provides a more conservative representation of the weld material strength. Nonetheless, the problem is pursued as though the weld material has its own stress-strain curve data in order to illustrate how three different materials would be handled.

The curve-strength ranking process at a given temperature is much more involved when multiple materials exist than when only one material exists (which allows a simple straightforward process, [25]). This is because the strength ranking of a given set of material curves can depend on the particular combination of material curves used for the other two materials (for example, wall strength and flexure can affect stress-strain phenomena at the weld notch). There are many such combinations because each of the two other materials has multiple material curves, so the ranking investigation should involve confirming curve ranking is robust over all or at least a few different test combinations of the other materials' curves. This was found in [9] to be true but for a single test exception.

Approximately 120 mechanical-only can-level simulations were performed in the material curves down-selection and strength ranking process. This work and MLEP material model calibrations were the most laborious and computationally expensive aspects of the PCAP VVUQ activity.

Step II *– Correlation and Interpolation of stress-strain curves across temperatures*

For each material, three curves for low, medium, and high effective strength exist per characterization temperature. When several material curves exist at each temperature, for UQ purposes strength is assumed to be highly correlated across temperatures such that a curve with higher relative strength at lower temperatures is assumed to retain higher relative strength at higher temperatures. This assumes that material weakening mechanisms and % weakening are roughly similar with increasing temperature whether the material is initially of higher, medium, or lower relative strength.

The correlation assumption appears physically reasonable and tremendously reduces the number of potential combinations of material curves to be sampled when a material transitions temperatures. For example, there are 3x3x3=27 potential combinations of material curve combinations in the figure that could be used in a simulation that transitions temperatures from 600ºC to 700ºC to 800ºC. So to investigate all these potential combinations would take 27 CompSim runs. To transition all seven temperatures would present $3^7 = 2187$ possible combinations. This is just for one material. For the three materials in this problem, each with three material curve options, this would present $2187^3 \approx 10^{10}$ possible combinations. Clearly this is unaffordable and seems wholly unnecessary given the reasonableness of the temperature-strength correlation assumption.

Hence, for each material, we link, e.g., its high-strength curves across the seven characterization temperatures. We interpolate across the seven characterization temperatures as follows. At a temperature in-between two adjacent characterization temperatures, the stress is linearly interpolated from the stress values (at the applicable input stain level) from the two stress-strain curves at the upper and lower enveloping temperatures. This effectively gives one constructed high-strength, temperature-varying, stress-strain function for each material. Temperature-dependent medium and low strength functions are likewise constructed. For this problem, we end up with each material having high strength (HS), medium strength (MS), and low strength (LS) temperature-dependent stress-strain functions as depicted in Figure 7.

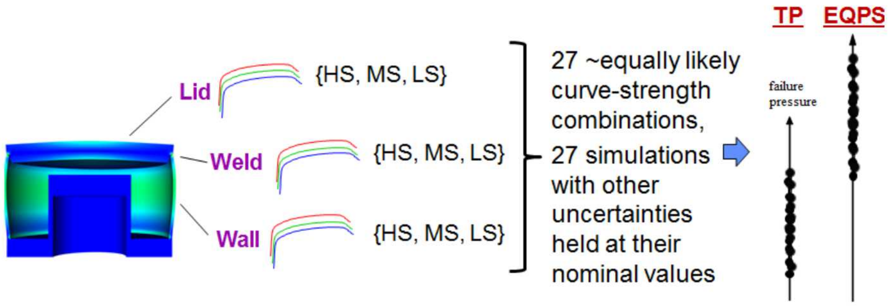

Figure 7. Notional depiction of PCAP can materials high strength (HS), medium strength (MS), and low strength (LS) temperature-dependent stress-strain functions, and propagation of the material strength variability via 27 assumed equally-likely combinations of material strength functions (e.g. one combination is lid MS function / weld HS function / wall LS function).

4.2 Stress-Strain Function Uncertainty Propagation and Results

Given the constructed high, medium, and low strength stress-strain functions for the materials, a strategy was taken to form and propagate all 27 possible combinations of stress-strain functions as conveyed in Figure 7. The model (Mesh 4) was run with experimental heating and other conditions from Test 6 in [14]. This is the reference nominal test of the five replicate tests in the PCAP validation assessment (see [12]). This yields 27 failure pressures for each the TP and the EQPS failure criteria as depicted in the figure. Quantitative results are presented in [9]. Briefly, the EQPS results are an average of about 460 *psi* or 50% higher than the TP failure pressures. (It was later determined that much of this difference could be explainable by very under-converged Mesh 4 results with the EPQP damage model, see [8].)

A sensitivity analysis in [9] shows that, for both failure criteria, the weld material strength variations have the largest effect, then the wall strength variations, then the lid strength variations. The lid was much thicker than the walls, so flexes and impacts the stress condition (and maximum stress) at the weld relatively little regardless of which lid-strength curve is used. Nevertheless, no material's strength variations have an insignificant effect.

We next consider the processing and interpretation of the pressure failure results. If dealing with multiple but few stress-strain curves for only one material, then appropriate uncertainty treatment has been established and confirmed in the series of papers and reports [26], [1], [4], [5]. The approach recognizes that the stress-strain curves are discrete realizations with no readily identifiable parametric relationship between them. Yet, the stress-strain (ss) curves come from and belong to a larger population that reflects the material's variability. Fortunately, a mathematical description of the generating function for the larger population of ss curves is not needed with the approach summarized next. The output scalar data (the predicted failure pressures) are worked with, rather than attempting to create a parametric or spectral generator function that is consistent with the ss curve data realizations.

An application of the approach with, say, three stress-strain function curves for a single material would result in three predicted failure pressures with the EQPS or TP failure criteria. (We could also work with other scalar output responses of interest, like displacement, strain, or Von Mises stress at a given point on the can and at a given time, or even spatial-temporal maxima as scalar quantities that vary with the three input stress-strain function curves.) Because only three function curves and corresponding failure pressure realizations exist, small-sample related error will typically exist in any characterization of aleatory uncertainty due to the stochastic material strength variability. Thus, substantial small-sample epistemic uncertainty exists concerning the error in characterizing the aleatory variability.

A small number of realizations or samples will usually under-predict the true variance of material strength and related failure pressures or other responses. Mean or central response will also usually be significantly mispredicted. Potential significant non-conservative small-sample bias error can result, causing unsafe engineering design and risk analysis, even if the physics prediction model is perfect in every other way.

Statistical Tolerance Intervals (TIs, e.g, [27]-[29]) attempt to compensate for sparse sample data by appropriately biasing response estimates. For instance, the three failure pressure values would be processed into 95%coverage/90%confidence TIs (95/90 TIs). With reasonably high reliability these estimate conservative but not overly conservative bounds on the "central" 95% of response from very sparse random samples/realizations of the input data. The central 95% of response is the range between the 2.5 and 97.5 percentiles of the true response distribution that would arise from an infinite number of samples. This central 95% range has been found to be convenient and meaningful for model validation comparisons of experimental and model-predicted aleatory response quantities (e.g., [25], [30]-[32]), which is also the purpose of the present UQ results.

Investigations in [2]-[5] have concluded 95/90 TIs to be preferable to many other UQ methods tried or critically assessed for estimating, from very sparse sample data, conservative but not overly conservative bounds on the central 95% of response. As reviewed in those documents, the other methods tried or critically evaluated include Bootstrapping, optimized four-parameter Johnson-family distribution fit to the response samples, non-parametric kernel density estimation specifically designed for sparse data, non-parametric cubic-spline probability density functions (PDF) fit to the data based on maximum likelihood, and Bayesian sparse-data approaches.

The TI approach is also much easier to use than the other UQ methods investigated. A 95/90 TI is constructed by simply multiplying the calculated standard deviation $\tilde{\sigma}$ of the data samples by a factor f to create an interval of total length $2f\tilde{\sigma}$. The interval is centered about the calculated mean $\tilde{\mu}$ of the samples. The multiplying factor f is readily available from tables in statistical texts (e.g. [28], [29]) or formulas (e.g. [27]), or available software (e.g. [33]) that encodes the formulas.

Although derived for Normal populations, 95/90 TIs will span the central 95% ranges of many other sparsely sampled PDF types with reasonable/useful odds or confidence. For instance, 89% of 144 PDFs (including highly skewed and multi-modal highly non-Normal distributions) studied in [1], [4], [5] had empirical confidence levels of 75% or greater with 95/90 TIs and N=4 random samples. From studies in [4] on several diverse PDFs, it is projected that 90% of the 144 PDFs would have confidence levels > 85% with 95/<u>95</u> TIs and N=4.[3] These average or expected confidence levels are shown to decline slowly as the number of samples increases.

Although TIs often provide reliably conservative estimates, TIs can egregiously exaggerate the true variability when very few samples are involved. This is a downside that comes with high confidence levels of bounding the true central 95% of response.

Incidentally, if the model predictions are to be used to support estimation of small "tail" probabilities of response for robust/reliable design or safety/risk analysis, the response samples would be processed in a different way. This is demonstrated in recent investigations in [4], [6], [35] on 16 diversely shaped distributions and tail probability magnitudes from 10^{-5} to 10^{-1}. Reliably conservative and efficient estimates of small tail probabilities are obtained. Further

---

[3] Confidence levels of 75% or 85% are often adequate to sufficiently manage risk, especially if conservatism from other sources exists in the analysis or results—such as when several sources of uncertainty are present where each involves sparse data conservatively treated with the TI method. Studies in [3] and [34] indicate that when more than one dominant or influential uncertainty sources are sparsely sampled and represented conservatively with TI confidence levels of say >70%, when the conservatively represented uncertainties are combined in linear propagation or aggregation, the individual conservative biases compound to yield substantially greater than 70% confidence of conservative bias in the combined uncertainty estimate.

reliability and accuracy benefits occur from averaging multiple estimates from equally legitimate subsets of samples from the available sparse-data pool (i.e., from use of statistical Jackknifing).

Now we consider the problem where the output response samples come from discrete stress-strain function variations of multiple materials as in the present problem. A naive approach would be to construct (e.g., 95/90) TIs from the 27 failure pressure values indicated in Figure 7 for the TP and EQPS failure criteria. However, TIs pertain to random sampling of the contributing input uncertainties, where for 27 response samples, each of the contributing source uncertainties would typically be sampled at 27 different values. Repeat values would not ordinarily occur, especially with a moderately small number of samples like 27. This is not the case here; each input stress-strain function of a given material is sampled repeatedly (nine times) in the course of propagating all possible combinations of curves. So it was decided that constructing TIs using n=27 would not be appropriate. (This was later supported by studies on a linear test problem in [34].) Instead, because only nine independent realizations of input information exist in this problem (three stress-strain functions for each of three materials), it was ventured that TIs should be constructed based on an effective number of samples N=9. Having no more-fundamental basis to proceed on at the time[4], this course was taken in the PCAP VVUQ project, as follows.

For an effective number of samples N=9, the multiplier factor for a 95/90 TI is $f = 3.125$. Multiplying this by the calculated standard deviations $\tilde{\sigma}_{TP} = 34.5$ psi and $\tilde{\sigma}_{EQPS} = 38.87$ psi of the 27 failure pressures calculated with TP and EQPS failure criteria yields TI half lengths $f\tilde{\sigma}$ are 107.8 psi for TP and 121.5 psi for EQPS. The respective TIs are centered at respective means $\tilde{\mu}_{TP} = 971.6$ psi and $\tilde{\mu}_{EQPS} = 1431.1$ psi of the 27 failure pressures for the two failure criteria. The TI upper and lower extents are located at the *upper end* $= \tilde{\mu} + f\tilde{\sigma} =$ (1079.3-TP; 1552.5-EQPS) psi and the *lower end* $= \tilde{\mu} - f\tilde{\sigma} =$ (863.9-TP; 1309.6-EQPS) psi.

For further uncertainty representation and analysis purposes, “Equivalent Normal” (EN) distributions are constructed such that their 2.5 and 97.5 percentiles coincide with the end points of the established 95/90 TIs. This is portrayed notionally in Figure 8. The TI EN distributions are defined by their mean and standard deviation parameters as:

$$\text{TI-EN}_{TP}(\tilde{\mu}_{TP} = 971.6 \text{ psi}; \tilde{\sigma}_{EN\text{-}TP} = 54.9 \text{ psi}) \quad (6)$$

$$\text{TI-EN}_{EQPS}(\tilde{\mu}_{EQPS} = 1431.1 \text{ psi}; \tilde{\sigma}_{EN\text{-}EQPS} = 62.0 \text{ psi}). \quad (7)$$

---

[4] There is a lack of well-established sampling methods for identifying combinations of model inputs from sparse quantized sets of choices or “levels” in the various factors (i.e., the levels are not prescribable; the few available stress-strain functions are the only “levels” available), such that propagation of the relatively small number of affordable or available input combinations will yield appropriate response statistics and distribution information. Subsequent to the PCAP project, investigations in [36] provide a more fundamentally grounded approach. As explained in [9], the approach would construct and average TIs based on failure pressure results from propagating selected sets of the 27 possible combinations of material curves. The selected sets would come from taking a Latin Hypercube Sampling (LHS [37]) analogue for the sampling and Monte Carlo (MC) propagation of ss curves from multiple materials. LHS is well recognized as an efficient sampling method [38] for Monte Carlo propagation of probabilistic uncertainty through general nonlinear response functions or models.

5. Convolution Aggregation of Uncertainties from Parametric and Discrete Aleatory Sources

Figure 8 depicts the conceptual idea of convolution to aggregate the separately propagated aleatory uncertainties defined by the material strength/failure variabilities represented by the TI ENs defined by Eqn. 6 or 7, and the PDF histograms shown in Tables 3-2, 3-3, 3-5, 3-6 arising from MC propagation of the three parametric uncertainties (Section 3). The random-sampling linear convolution procedure is explained next.

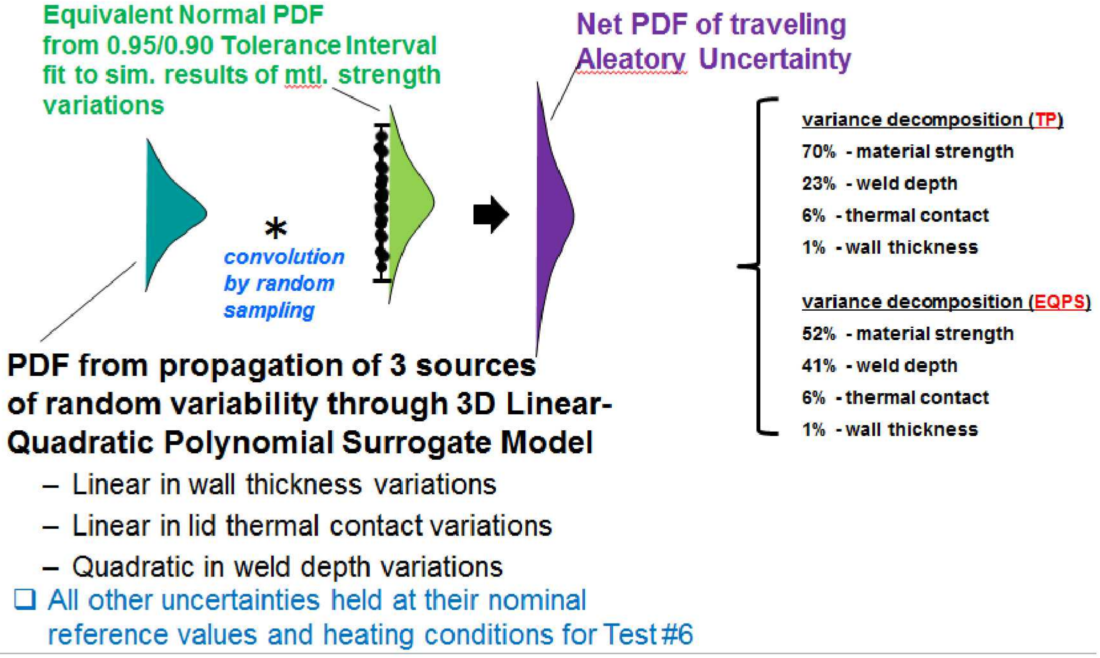

Figure 8. Net PDF of failure pressure random variability and associated contribution sensitivities from aggregation of resultant PDF of propagated parametric random variables and Equivalent Normal PDF of material strength variability effects.

The convolution procedure treats the EN response PDF from material variability effects, and the response PDF due to the continuous parametric sources, as being independent PDFs. It furthermore treats the PDFs' samples/realizations relative to some nominal response value r^0 as perturbations that linearly add or *superpose* into a combined perturbation due to material variability + parametric geometry and contact heat-transfer temperature effects:

$$r_{conv}^{i} = r^{0} + \Delta r_{P}^{i}|\vec{f}_{D}^{0} + \Delta r_{D}^{i}|\vec{x}_{P}^{0} \qquad (8)$$

where

r_{conv}^{i} = a sample or realization of the combined (convolved) uncertainty from propagation of the parametric uncertainty U[$\vec{x}_P$] (where the vector notation denotes multiple parametric uncertainty sources) and the discrete uncertainty U[$\vec{f}_D$] (here denoting uncertainty from multiple discrete stress-strain curve function realizations from replicate tests for each of multiple sources (multiple materials));

$r^{0} = r(\vec{x}_{P}^{0}, \vec{f}_{D}^{0})$ is the nominal response value (here failure pressure) yielded by the model given nominal input values of the discrete and parametric uncertainties (e.g., Eqn. 4 in Section 3) where $r(\vec{x}_P, \vec{f}_D)$ represents the model's output failure pressure variation as a function of the said inputs);

$r_{P}^{i}|\vec{f}_{D}^{0}$ is a sample from the response PDF obtained by propagating the parametric uncertainty U[$\vec{x}_P$] while holding the discrete uncertainty realizations to a nominal set $\vec{f}_{D}^{0}$ (e.g., the PDFs plotted in Tables 3-2, 3-3, 3-5, 3-6, generically designated PDF$_r$(U[$\vec{x}_P$], $\vec{f}_{D}^{0}$));

$r_{D}^{i}|\vec{x}_{P}^{0}$ is a sample from the response PDF obtained by propagating the discrete uncertainty U[$\vec{f}_D$] while holding the parametric uncertainties at nominal values $\vec{x}_{P}^{0}$ (the PDFs defined by Eqns. 6 and 7, generically designated PDF$_r$($\vec{x}_{P}^{0}$, U[$\vec{f}_D$]));

$$\Delta r_{P}^{i}|\vec{f}_{D}^{0} = r_{P}^{i}|\vec{f}_{D}^{0} - r^{0}\,; \qquad (9)$$

$$\Delta r_{D}^{i}|\vec{x}_{P}^{0} = r_{D}^{i}|\vec{x}_{P}^{0} - r^{0}. \qquad (10)$$

A simplified illustrative example of linear convolution is presented below. The validity of linear convolution in the PCAP problem depends on the following conditions.

- Independence exists between the material variability uncertainty sources that underlie the Equivalent Normal failure-pressure response PDFs defined by Eqn. 6 or 7, and the three geometry and heat-transfer related source uncertainties (PDFs) underlying the failure-pressure response PDFs in Tables 3-2, 3-3, 3-5, 3-6. It is judged that this condition is well met in the current problem.
- The resultant PDFs (Eqns. 6 and 7 and those in Tables 3-2, 3-3, 3-5, 3-6) are as well independent from each other if there are no response interactions when the material variability uncertainty sources are taken together with the geometry/heat-transfer uncertainty sources. This occurs when response is linear over the joint uncertainty space of all the source uncertainties, or when a slightly relaxed condition exists as exemplified in the example below and stated mathematically in Figure 9. Either case would result in the following. If the three geometry/heat-transfer uncertainty sources were propagated with material strength functions other than the nominal median-strength ones used in

> Section 3, the response PDFs shown in Tables 3-2, 3-3, 3-5, 3-6 would change location along the abscissa, <u>but not change shape</u>. Similar considerations apply for the TI-EN response PDFs from material strength variability if propagation of the material curves in Section 4 occurred under values of the continuous parametric uncertainties other than the nominal ones used. It is often the case that approximately linear behavior exists in model calibration and validation activities over the small ranges of the input uncertainties in these activities—which endeavor to reduce or control experimental and simulation uncertainties to small magnitudes. In the PCAP VVUQ problem, any interactions are judged to be small and to have negligible effect relative to the other sources of uncertainty and numerical precision error in the problem. This was not checked or confirmed because of time and resource constraints in the project—but normally should be checked in project work if possible.

Note that these restrictions do not exclude interactions within the set of continuous parametric variables or within the set of discretely represented random variables or functions. Nor are correlations restricted within the set of parametric variables or within the set of discrete random inputs. However, there must be no (or insignificant) interactions and correlations between the two groups of variables (over their uncertainty ranges).

Figure 9 presents a simple example illustrating generation of random samples r_{conv}^{i} for constructing the combined output distribution by linear convolution. The random-variable input uncertainties are characterized by a continuous distribution PDF_{x_P} = U$[x_P]$ for input variable x_P and three samples $\{x_D^i\}$ that discretely characterize uncertainty U$[x_D]$ (e.g., an otherwise unspecified continuous random variable) for input variable x_D.

Consider a random sample x_P^i from PDF_{x_P} as indicated in the figure. Pair this sample realization with the three realizations $\{x_D^i\}$ of the discretely characterized uncertainty to evaluate the model (response function $r(x_P,x_D)$) at these variable combinations and obtain the three realizations of response as shown. Thus, the discretely represented random variability is propagated conditional on the particular sample value x_P^i from the continuous PDF uncertainty source. The corresponding dashed blue distribution on the response axis, PDF$_r$(x_P^i, U$[x_D]$), signifies an Equivalent-Normal PDF from a 95/90 tolerance interval based on the three response samples. Note that this TI-EN PDF has the same shape that would be obtained if the process is applied for a different sample and value $x_P^{i}{}'$ from PDF_{x_P}. This occurs when no interactions exist between variables with discrete vs. continuous uncertainty representation, either for a linear response function $r(x_P,x_D)$ or for one with slightly relaxed conditions per the equation at top-right in Figure 9.

A random sample from the TI-EN PDF$_r$(x_P^i, U$[x_D]$) is marked by the green square on the response axis in the figure. Its value is denoted r_{conv}^{i}; it is a combined result of propagated effects of a random sample from the continuous input uncertainty source PDF_{x_P} and added effect of a random sample of response uncertainty inferred from propagated discrete samples of the otherwise unspecified continuous input source uncertainty U$[x_D]$. A resultant distribution of the two effects combined can be constructed by generating many such r_{conv}^{i} samples from randomized replication of the presented process.

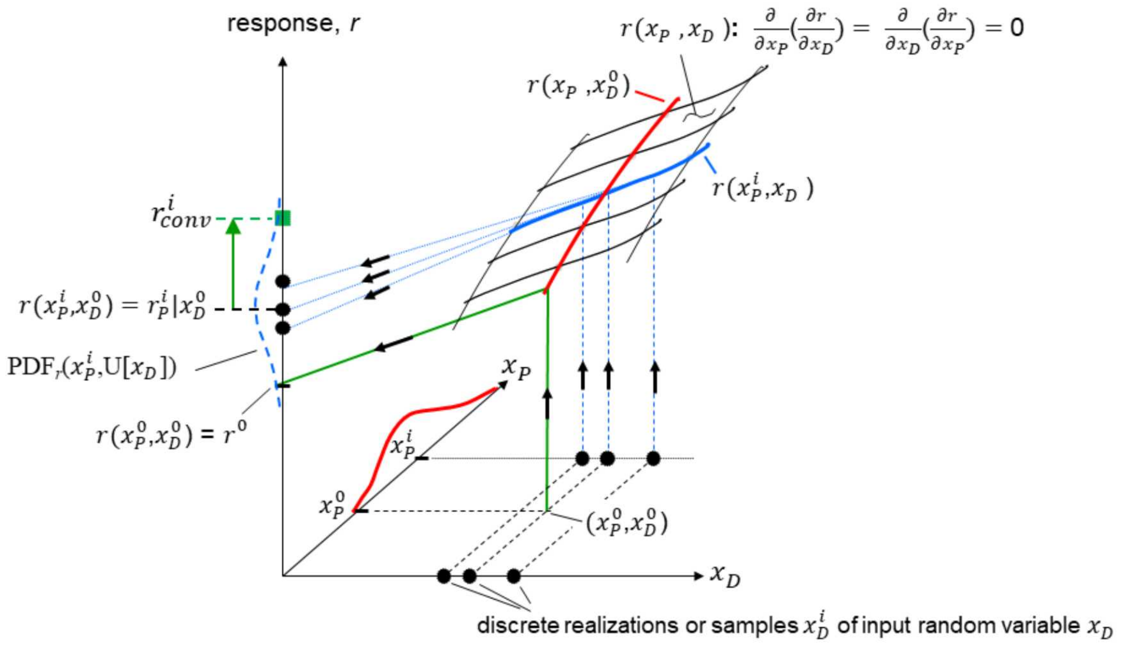

Figure 9. Simple example illustrating generation of random samples r_conv^i for constructing the combined output distribution by linear convolution.

Note that the illustrated process is consistent with Eqn. 8 as follows. Substituting Eqn. 9 into 8 yields

$$r_{conv}^i = r_P^i|\vec{f}_D^0 + \Delta r_D^i|\vec{x}_P^0. \tag{11}$$

Writing this in terms of the simplified quantities in the illustrative problem gives

$$r_{conv}^i = r_P^i|x_D^0 + \Delta r_D^i|x_P^0. \tag{12}$$

The first term on the right side (RS) of Eqn. 12 is identified on the response axis in Figure 9. The last term on the RS of Eqn. 12 is a perturbation defined by a special case of Eqn. 10:

$$\Delta r_D^i|x_P^0 = r_D^i|x_P^0 - r^0. \tag{13}$$

The RS of Eqn. 13 must be shown to be equivalent to the perturbation signified by the green arrow in the figure (near the response axis) in order for the geometric construction underlying the figure to be consistent with Eqn. 12 as a reduced special case of the general relation Eqn. 8 obtained by different geometric reasoning. The magnitude and direction of the green arrow is defined by the difference A) below. This difference is the same as in B) corresponding to Eqn.

13. The equivalency proceeds from the specified condition at the top-right of Figure 9 that ensures all TI-EN PDFs have the same shape when generated from the three propagated input samples $\{x_D^i\}$ when propagated for any set value x_P^i of the parametric uncertainty. Thus, the equivalence sought at the start of this paragraph is established.

A) [response value of a sample from the dashed blue TI-EN PDF$_r$(x_P^i, U[x_D]) on the response axis] minus [response value $r_P^i|x_D^0$ of the middle of the three propagated discrete samples propagated while holding the parametric uncertainty at a value x_P^i]

B) [response value $r_D^i|x_P^0$ of a sample at the same quantile as in A) but from a <u>shifted</u> same-shaped distribution PDF$_r$(x_P^0, U[x_D])] minus [response value $r_P^0|x_D^0 = r^0$ of the middle of the three propagated discrete samples propagated while holding the parametric uncertainty at a value x_P^0]

The PCAP work used the form Eqn. 11. The first term on its RS corresponds to a sample from the PDFs in Tables 3-2, 3-3, 3-5, or 3-6. The other term in Eqn. 11's RS is defined by Eqn. 9. In analogy with B) above, the first term on the RS of Eqn. 9 is a sample from the TI-EN PDF in Eqn. 6 or 7. The value r^0 in Eqn. 9 is found in columns J of Tables 3-2, 3-3, 3-5, 3-6. The resultant convolution histograms are shown in Figure 10. The histograms were constructed with 10,000 r_{conv}^i samples. The shapes of the histograms are reasonably close to Gaussian. This allows the histograms to be well approximated by Normal PDFs for representational convenience in [11], [12].

TP-linear RSA	**TP-lin+quadrat RSA**	**EQPS-linear RSA**	**EQPS-lin+quadrat RSA**
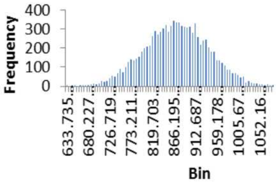	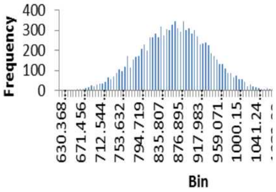	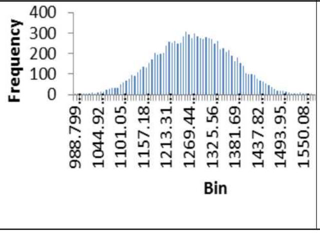	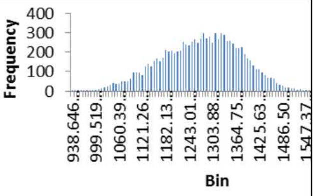

Figure 10. Histograms of convolved response effects from parametric and discrete aleatory input uncertainties.

Statistics of the histograms and their Normal approximations are given in Table 5-1. Note that the Normal approximations are developed using the 2.5 and 97.5 percentiles of the histograms, instead of using the histogram means and standard deviations. This is thought to better cover the uncertainty of non-symmetric distributions like the last one in Figure 10. The means and standard deviations of the histograms are included in Table 5-1 to compare against the derived means using the histogram 2.5 and 97.5 percentiles. The histogram means and their percentile-derived counterparts are within 0.4% of each other in all four cases (rows of the table). The analogous differences for standard deviations vary from a minimum of 0.8% to a maximum of 3.2%.

Table 5-1. Statistics of Convolved Response from Parametric and Discrete Aleatory Input Uncertainties.

case	2.5%ile	97.5%ile	mean	stdev	Equivalent-Normal mean	Equivalent-Normal stdev
TP-linear RSA	738.9	1008.4	868.9	69.6	873.6	68.7
TP-lin+quadrat RSA	730.7	1009.9	867.0	71.8	870.3	71.2
EQPS-linear RSA	1106.6	1459.8	1277.7	92.3	1283.2	90.1
EQPS-lin+quadrat RSA	1070.6	1461.6	1270.7	102.9	1266.1	99.7

The sensitivity contributions of the net aggregated uncertainty for the linear+quadratic results are listed in Figure 8. These numbers come from row 10,016 of Tables 3-5 and 3-6. For linear and linear+quadratic results and both EQPS and TP failure criteria, material strength variability contributes the most to failure pressure variability, followed by weld depth variability, thermal contact temperature-effect variability, and wall thickness variability.

6. Conclusion

This paper presented a practical, versatile, and effective methodology for propagating and combining the effects of random variations of several continuous scalar quantities and several random-function quantities. It was explained how to effectively propagate the material stress-strain curve-to-curve discrete variations and appropriately account for the small sample size of the functional data realizations. This was coordinated with the propagation of random-variable PDFs of three continuous parametric scalar uncertainties. Motivated by the high expense of the physics model simulations, a simple dimension- and order- adaptive polynomial response surface approach was used to propagate the effects of the random variables and enable uncertainty estimates on the error contributed by using the surrogate model. Linear convolution was used to aggregate the resultant aleatory uncertainty from the parametrically propagated random variables with an appropriately conservative probability distribution of aleatory effects from propagating the multiple stress-strain curves for each material. The response surface constructions and their Monte Carlo sampling for uncertainty propagation, and linear sensitivity analysis and convolution procedures, were demonstrated with standard EXCEL spreadsheet functions, attesting to the relative simplicity and practicality of the versatile and effective propagation and aggregation methodology.

7. References

[1] Romero, V., J.F. Dempsey, B. Schroeder, J. Lewis, N. Breivik, G. Orient, B. Antoun, J. Winokur, M. Glickman, J. Red-Horse, "Evaluation of a Simple UQ Approach to Compensate for Sparse Stress-Strain Curve Data in Solid Mechanics Applications," 19th AIAA Non-Deterministic Approaches Conference, paper AIAA2017-0818, AIAA SciTech 2017, Jan. 9-13, Grapevine, TX.

[2] Romero, V., J. Mullins, L. Swiler, A. Urbina, "A Comparison of Methods for Representing and Aggregating Experimental Uncertainties involving Sparse Data—More Results," article 2013-01-0946, *Soc. Automot. Engrs. Int. J. of Materials and Manufacturing*, vol. 6 (no. 3), 2013, pp. 447-473, doi:10.4271/2013-01-0946.

[3] Romero, V., L. Swiler, A. Urbina, J. Mullins, "A Comparison of Methods for Representing Sparsely Sampled Random Quantities," Sandia National Laboratories report SAND2013-4561 printed September 2013.

[4] Romero, V., M. Bonney, B. Schroeder, V.G. Weirs, "Evaluation of a Class of Simple and Effective Uncertainty Methods for Sparse Samples of Random Variables and Functions," Sandia National Laboratories report SAND2017-12349, Nov. 2017.

[5] Romero, V., B. Schroeder, J.F. Dempsey, N. Breivik, G. Orient, B. Antoun, J.R. Lewis, J. Winokur, "Simple Effective Conservative Treatment of Uncertainty from Sparse Samples of Random Variables and Functions," *ASCE-ASME Journal of Uncertainty and Risk in Engineering Systems: Part B. Mechanical Engineering*, DOI 10.1115/1.4039558, Dec. 2018, vol. 4, pp. 041006-1 – 041006-17.

[6] Jekel, C., and V. Romero, "Bootstrapping and Jackknife Resampling to Improve Sparse-Data UQ Methods for Tail Probability Estimates with Limited Samples," ASME paper VVS2019-5127, ASME 2019 Verification and Validation Symposium VVS2019, May 15-17, 2019, Las Vegas, NV.

[7] Black, A., Romero, V., Breivik, N., Orient, G., Antoun, B., Dodd, A., Suo-Anttila, J., 2019, "Predictive Capability Assessment Project: Abnormal Thermal-Mechanical Breach V&V/UQ," Sandia National Laboratories report SAND2019-13790, November 2019.

[8] Black, A., Romero, V., Breivik, N., Orient, G., Suo-Anttila, J., Antoun, B., Dodd, A., "Verification, Validation, and Uncertainty Quantification of a Thermal-Mechanical Pressurization and Breach Application," presentation VVS2015-8047 in the archives of the ASME Verification & Validation Symposium, May 13-15 2015, Las Vegas, NV.

[9] Romero, V., Black, A., Orient, G., Antoun, B., "Propagating Stress-Strain Curve Variability in Multi-Material Problems: Temperature-Dependent Material Tests to Plasticity Models to Structural Failure Predictions," Sandia National Laboratories document SAND2019-13095 O, Oct. 2019, and chapter for *Engineering Failure Analysis*, Intech Open Publishers (in press, 2019).

[10] Romero, V., and Black, A., "Processing of Random and Systematic Experimental Uncertainties for Real-Space Model Validation involving Stochastic Systems," to be submitted to *ASME J. Verification, Validation, and Uncertainty Quantification.*

[11] Romero, V., and Black, A., "Adaptive Polynomial Response Surfaces and Level 1 Probability Boxes for Propagating and Representing Aleatory and Epistemic Components of Uncertainty in Model Validation," Sandia National Laboratories document in review (2019).

[12] Romero, V., Black, A., Dodd, A., Orient, G., Breivik, N., Antoun, B., Suo-Anttila, J., 2019, "Real-Space Model Validation-UQ Methodology and Assessment for Thermal-Chemical-Mechanical Response and Weld Failure in Heated Pressurizing Canisters," to be submitted to *ASME J. Verification, Validation, and Uncertainty Quantification.*

[13] Antoun, B. R., 2012, "Material Characterization and Coupled Thermal-Mechanical Experiments for Pressurized, High Temperature Systems," Sandia National Laboratories, Livermore, CA, Technical Report.

[14] Suo-Anttila, J.M., Dodd, A.B., Jernigan, D.A., "Thermal Mechanical Exclusion Region Barrier Breach Foam Experiments (800C Upright and Inverted 20 lb/ft3 PMDI Cans)," Sandia National Laboratories report SAND2012-7600 (OUO/ECI), September 2012.

[15] Wellman, G. W., "A Simple Approach to Modeling Ductile Failure," Sandia National Laboratories report SAND 2012-1343, 2012.

[16] Sierra/SM Development Team, "Sierra/SM Theory Manual," Sandia National Laboratories report SAND2013-4615, July 2013.

[17] Breivik, N., "Laser Weld Modeling Methods for Deformation and Failure," Sandia National Laboratories Internal Memorandum to Amalia Black, Albuquerque, New Mexico, September 9, 2011.

[18] Notz, P.K., Subia, S.R., Hopkins, M.M., Moffat, H.K., Nobel, D.R., "Aria 1.5: user manual," Sandia National Laboratories report SAND2007-2734, April 2007.

[19] Erickson, K.L., Dodd, A.B., and Hogan, R.E., "Modeling Pressurization Caused by Thermal Decomposition of Highly Charring Foam in Sealed Containers," Proceedings of BCC 2010, Stamford, CT, 23-26 May 2010.

[20] Edwards, H. C., and Stewart, J. R., "SIERRA: A Software Environment for Developing Complex Multi-Physics Applications." In First MIT Conference on Computational Fluid and Solid Mechanics, edited by K. J. Bathe, 1147–1150. Amsterdam: Elsevier, 2001.

[21] Larsen, M.E. and Dodd, A.B., "Modeling and Validation of the Thermal Response of TDI Encapsulating Foam as a Function of Initial Density," Sandia National Laboratories report SAND2014-17850, September 2014.

[22] Saltelli, A., Tarantola, S., Campolongo, F., Ratto, M., Sensitivity Analysis in Practice: A Guide to Assessing Scientific Models. New York: Wiley; 2004.

[23] Helton, J.C., J.D. Johnson, C.J. Sallaberry, C.B. Storlie, "Survey of Sampling-Based Methods for Uncertainty and Sensitivity Analysis," Sandia National Laboratories report SAND 2006-2901, June 2006.

[24] Swiler, L.P., V.J. Romero, "A Survey of Advanced Probabilistic Uncertainty Propagation and Sensitivity Analysis Methods," Chapter 6 of Joint Army/Navy/NASA/Air Force (JANNAF) e-book: Simulation Credibility—Advances in Verification, Validation, and

Uncertainty Quantification, U. Mehta (Ed.), D. Eklund, V. Romero, J. Pearce, N. Keim, document NASA/TP-2016-219422 and JANNAF/GL-2016-0001, Nov. 2016.

[25] Romero, V., F. Dempsey, B. Antoun, "Application of UQ and V&V to Experiments and Simulations of Heated Pipes Pressurized to Failure," Chapter 11 of Joint Army/Navy/NASA/Air Force (JANNAF) e-book: *Simulation Credibility—Advances in Verification, Validation, and Uncertainty Quantification*, U. Mehta (Ed.), D. Eklund, V. Romero, J. Pearce, N. Keim, document NASA/TP-2016-219422 and JANNAF/GL-2016-0001, Nov. 2016.

[26] Romero, V., J.F. Dempsey, G. Wellman, B. Antoun, "A Method for Projecting Uncertainty from Sparse Samples of Discrete Random Functions ─ Example of Multiple Stress-Strain Curves," paper AIAA-2012-1365, 14th AIAA Non-Deterministic Approaches Conference, April 23-26, 2012, Honolulu, HI.

[27] Howe, W. G. (1969). "Two-sided Tolerance Limits for Normal Populations - Some Improvements", Journal of the American Statistical Association, 64, pages 610-620.

[28] Hahn, G.J., and Meeker, W.Q., *Statistical Intervals—A Guide for Practitioners*, Wiley & Sons, 1991.

[29] Montgomery, D.C., and Runger, G.C., *Applied Statistics and Probability for Engineers*, Wiley & Sons, 1994.

[30] Jamison, R., V. Romero, M. Stavig, T. Buchheit, C. Newton, "Experimental Data Uncertainty, Calibration, and Validation of a Viscoelastic Potential Energy Clock Model for Inorganic Sealing Glasses," presented at ASME Verification & Validation Symposium, Las Vegas, NV, May 18-20, 2016.

[31] Romero, V., R. Heaphy, B. Rutherford, J.R. Lewis, "Uncertainty Quantification and Model Validation for III-V SSICs in Annular Core Research Reactor Shots," Sandia National Laboratories report SAND2016-11772 (Official Use Only/Export Controlled), November 2016.

[32] Romero, V., "Real-Space Model Validation and Predictor-Corrector Extrapolation applied to the Sandia Cantilever Beam End-to-End UQ Problem," paper AIAA-2019-1488, 21st AIAA Non-Deterministic Approaches Conference, AIAA SciTech 2019, Jan. 7-11, San Diego, CA.

[33] Young, D.S. (2010). "Tolerance: An R Package for Estimating Tolerance Intervals." Journal of Statistical Software, 36(50), pp. 1-39.

[34] Winokur, J., and V. Romero, "Optimal Design of Computer Experiments for Uncertainty Quantification with Sparse Discrete Sampling," Sandia National Laboratories document SAND2016-12608, 2016.

[35] Jekel, C., and V. Romero, "Conservative Estimation of Tail Probabilities from Limited Sample Data," Sandia National Laboratories report in review (2019).

[36] Romero, V., J. Winokur, G. Orient, J.F. Dempsey, "Confirmation of Discrete-Direct Calibration and Uncertainty Propagation approach for Multi-Parameter Plasticity Model

Calibrated to Sparse Random Field Data," presentation VVS2019-5172 in the archives of the ASME Verification & Validation Symposium, May 15-17, 2019.

[37] Conover, W.J., "On a Better Method for Selecting Values of Input Variables for Computer Codes," 1975. unpublished manuscript recorded as Appendix A of "Latin Hypercube Sampling and the Propagation of Uncertainty Analysis of Complex Systems" by J.C. Helton and F.J. Davis, Sandia National Laboratories report SAND2001-0417 printed November 2002.

[38] McKay, M.D., R.J. Beckman, W.J. Conover, "A Comparison of Three Methods for Selecting Values of Input Variables in the Analysis of Output from a Computer Code," *Technometrics*, Vol. 21, no. 2, 1979.

[39] Orient, G.E., and Mersch, J.P., "Multilinear Elastic-Plastic Constitutive Calibrations Supporting UQ for Al 5083, Al 7079, Al 6061T651, Al 7075T651 Alloys," Sandia National Laboratories report SAND2018-7198, July 2018.